Acta Neuropathol (2008) 115:561–575
DOI 10.1007/s00401-007-0329-z

ORIGINAL PAPER

Basophilic inclusion body disease and neuronal intermediate filament inclusion disease: a comparative clinicopathological study

Osamu Yokota · Kuniaki Tsuchiya · Seishi Terada · Hideki Ishizu · Hirotake Uchikado · Manabu Ikeda · Kiyomitsu Oyanagi · Imaharu Nakano · Shigeo Murayama · Shigetoshi Kuroda · Haruhiko Akiyama

Received: 19 October 2007 / Revised: 30 November 2007 / Accepted: 1 December 2007 / Published online: 13 December 2007

Abstract While both neuronal intermediate filament inclusion disease (NIFID) and basophilic inclusion body disease (BIBD) show frontotemporal lobar degeneration and/or motor neuron disease, it remains unclear whether, and how, these diseases differ from each other. Here, we compared the clinicopathological characteristics of four BIBD and two NIFID cases. Atypical initial symptoms included weakness, dysarthria, and memory impairment in BIBD, and dysarthria in NIFID. Dementia developed more than 1 year after the onset in some BIBD and NIFID cases. Upper and lower motor neuron signs, parkinsonism, and parietal symptoms were noted in both diseases, and involuntary movements in BIBD. Pathologically, severe caudate atrophy was consistently found in both diseases. Cerebral atrophy was distributed in the convexity of the fronto-parietal region in NIFID cases. In both BIBD and NIFID, the frontotemporal cortex including the precentral gyrus, caudate nucleus, putamen, globus pallidus, thalamus, amygdala, hippocampus including the dentate gyrus, substantia nigra, and pyramidal tract were severely affected, whereas lower motor neuron degeneration was minimal. While α-internexin-positive inclusions without cores were found in both NIFID cases, one NIFID case also had α-internexin- and neurofilament-negative, but p62-positive, cytoplasmic spherical inclusions with eosinophilic p62-negative cores. These two types of inclusions frequently coexisted in the same neuron. In three BIBD cases, inclusions were tau-, α-synuclein-, α-internexin-, and neurofilament-negative, but

O. Yokota · K. Tsuchiya · H. Akiyama
Department of Neuropathology,
Tokyo Institute of Psychiatry,
2-1-8 Kamikitazawa, Setagaya-ku,
Tokyo 156-8585, Japan

O. Yokota (✉) · S. Terada · H. Ishizu · S. Kuroda
Department of Neuropsychiatry,
Okayama University Graduate School of Medicine,
Dentistry and Pharmaceutical Sciences,
2-5-1 Shikata-cho, Okayama 700-8558, Japan
e-mail: oyokota1@yahoo.co.jp

K. Tsuchiya
Department of Laboratory Medicine and Pathology,
Tokyo Metropolitan Matsuzawa Hospital, Tokyo, Japan

K. Tsuchiya
Department of Neurology,
Tokyo Metropolitan Matsuzawa Hospital, Tokyo, Japan

H. Ishizu
Department of Laboratory Medicine,
Zikei Institute of Psychiatry, Okayama, Japan

H. Uchikado
Department of Psychiatry,
Yokohama City University School of Medicine,
Yokohama, Japan

M. Ikeda
Department of Psychiatry and Neuropathobiology,
Kumamoto University Graduate School of Medical Sciences,
Kumamoto, Japan

K. Oyanagi
Department of Neuropathology,
Tokyo Metropolitan Institute for Neuroscience, Tokyo, Japan

I. Nakano
Division of Neurology, Department of Medicine,
Jichi Medical University School of Medicine, Tochigi, Japan

S. Murayama
Department of Neuropathology,
Tokyo Metropolitan Institute of Gerontology, Tokyo, Japan

occasionally p62-positive. These findings suggest that: (1) the clinical features and distribution of neuronal loss are similar in BIBD and NIFID, and (2) an unknown protein besides α-internexin and neurofilament may play a pivotal pathogenetic role in at least some NIFID cases.

Keywords α-Internexin · Caudate nucleus · Frontotemporal dementia · TDP-43 · Motor neuron disease

Introduction

Basophilic inclusion body disease (BIBD) is a rare disease entity, whose clinical phenotype includes dementia and motor neuron disease (MND) [25]. Cases of dementia having basophilic inclusions were originally called "generalized variant of Pick's disease" [24]. The clinical and pathological features of BIBD were reported to be young onset, remarkable degeneration in the frontotemporal cortex, caudate nucleus, and substantia nigra, and the occurrence of round cytoplasmic basophilic inclusions immunonegative for tau or neurofilament. As far as we know, only seven autopsy cases of generalized variant of Pick's disease have been reported [11, 14, 24, 36]. Like the generalized variant of Pick's disease, the onset age in MND cases with basophilic inclusions reported previously is very young, often under 40 years. MND with basophilic inclusions is also very rare, and only about ten cases of this subtype have been reported [1, 13, 18, 19, 22, 23, 28, 30, 33, 34, 37, 41].

Recently, a new disease entity of frontotemporal lobar degeneration (FTLD) called neuronal intermediate filament inclusion disease (NIFID), neurofilament inclusion body disease (NIBD), or neurofilament inclusion disease (NFID) was proposed [5, 6, 16]. A pathological hallmark of NIFID is the occurrence of neurofilament-positive intraneuronal inclusions. More recently, it was reported that α-internexin immunohistochemistry reveals the inclusions more sensitively and specifically [6, 39].

The morphological features of the inclusions in NIFID on conventional stains are quite similar to those of inclusions in BIBD. Further, the BIBD cases previously reported were not always fully examined immunohistochemically. Therefore, the clinical and pathological characteristics in BIBD have not been fully established, and whether the clinicopathological features of BIBD are different from those of NIFID remains unclear. In the present study, we first used α-internexin and neurofilament immunohistochemistry to differentiate NIFID cases from our series of cases that were previously diagnosed as BIBD, based on conventional stains. Then, we compared the clinical features, distribution of neuronal loss, and immunohistochemical characteristics of BIBD and NIFID cases.

Materials and methods

Subjects

Six cases previously diagnosed as BIBD were selected from our autopsy series. A diagnosis of BIBD had been made based on the conventional histopathological features of basophilic inclusion bodies reported previously: (1) round or oval intraneuronal inclusions that are detected by hematoxylin-eosin (H&E), Klüver-Barrera, and Bodian stains according to previous reports [24] and (2) that are not immunolabeled with antibodies against tau, α-synuclein, or ubiquitin. The six cases were immunohistochemically reexamined.

Neuropathological examination

Brain tissue samples from all subjects were fixed postmortem with 10% formalin and embedded in paraffin. Sections (10 μm thick) from the frontal, temporal, parietal, occipital, insular, and cingulate cortices, hippocampus, amygdala, basal ganglia, midbrain, pons, medulla oblongata, cerebellum, and spinal cord were prepared. These sections were stained by the hematoxylin-eosin (H&E), Klüver-Barrera, Holzer, methenamine silver, Bodian, and Gallyas-Braak methods.

Sections from representative regions of the cerebrum, brainstem, and spinal cord were examined immunohistochemically using antibodies to ubiquitin (Z0458, rabbit, polyclonal, 1:5,000, Dako, Glostrup, Denmark), ubiquitin (MAB1510, mouse, monoclonal, 1:500, Chemicon, Burlingame, CA, USA), phosphorylated tau (AT8, mouse, monoclonal, 1:3,000, Innogenetics, Ghent, Belgium), phosphorylated neurofilament (SMI31, mouse, monoclonal, 1:1,000, Sternberger, Lutherville, MD, USA), phosphorylation-independent neurofilament (SMI32: mouse, monoclonal, 1:100, Sternberger Monoclonals, Baltimore, MD, USA), α-internexin (ab32306, rabbit, polyclonal, 1:100, Abcam Plc., Cambridge, UK), phosphorylated α-synuclein (psyn#64, mouse, monoclonal, 1:1,000, Wako, Osaka, Japan), TDP-43 (10782-1-AP, rabbit, polyclonal, 1:500, ProteinTech Group Inc., Chicago, IL, USA), N-terminus of p62 protein (p62-N, guinea pig, polyclonal, 1:500, Progen Biotechnik GmbH, Heidelberg, Germany), C-terminus of p62 protein (p62-C, guinea pig, polyclonal, 1:500, Progen Biotechnik GmbH), polyglutamine (1C2, mouse, monoclonal, 1:10,000, Chemicon, Burlingame, CA, USA), and glial fibrillary acidic protein (GFAP, rabbit, polyclonal, 1:5,000, Dako). Deparaffinized sections were incubated with 1% H_2O_2 in methanol for 20 min to eliminate endogenous peroxidase activity in the tissue. Sections were treated with 0.2% TritonX-100 for 5 min and washed in phosphate-buffered saline (PBS, pH 7.4). When using anti-ubiquitin, anti-neurofilament,

anti-N-terminus p62, anti-C-terminus p62, and anti-α-internexin antibodies, the sections were pretreated by autoclaving for 10 min in 10 mM sodium citrate buffer at 120°C. After blocking with 10% normal serum, the sections were incubated for 72 h at 4°C with one of the primary antibodies in 0.05 M *Tris*–HCl buffer, pH 7.2, containing 0.1% Tween and 15 mM NaN_3. After three 10-min washes in PBS, the sections were incubated in biotinylated anti-rabbit, anti-mouse, or anti-guinea pig secondary antibody for 1 h, and then in avidin-biotinylated horseradish peroxidase complex (ABC Elite kit, Vector, Burlingame, CA, USA) for 1 h. The peroxidase labeling was visualized with 0.2% 3,3′-diaminobenzidine (DAB) as the chromogen. The sections were counterstained with hematoxylin. For double staining with N-terminal-specific p62 antibody (p62-N) and anti-α-internexin antibody (ab32306), primary antibody labeling in the first cycle (p62-N) was detected in the same way as single staining except that the DAB reaction was intensified with nickel ammonium sulfate to yield a dark purple precipitate. Then, primary antibody labeling in the second cycle (ab32306) was detected in the same way as single staining. The sections were counterstained with nuclear fast red for double immunostaining.

Semiquantitative assessment of histopathological lesions

Neuronal loss and gliosis in representative regions were semiquantitatively evaluated. The degree of degeneration in the cerebral cortex was assessed on H&E-, KB-, and GFAP-stained sections according to the following grading system employed in our previous study [43]: −, no histopathological alteration; +, slight neuronal loss and gliosis are observed only in the superficial layers; ++, obvious neuronal loss and gliosis are found in cortical layers II and III, and status spongiosis and relative preservation of neurons in layers V and VI are often present; and +++, pronounced neuronal loss with gliosis is found in all cortical layers, and the adjacent subcortical white matter exhibits prominent fibrous gliosis. In the basal ganglia and brainstem nuclei, the degree of neuronal loss and gliosis was assessed on H&E-, KB-, and GFAP-stained sections according to the following grading system: -, neither neuronal loss nor gliosis is observed; ±, mild gliosis is observed on H&E- or GFAP-immunostained sections, but neurons are not reduced in number; +, mild gliosis and mild neuronal loss are present; ++, neuronal loss and gliosis are moderate, but tissue rarefaction is absent; and +++, severe neuronal loss, severe fibrous gliosis, and tissue rarefaction are observed. Degeneration of the corticospinal tract at the level of the cerebral peduncle and medulla oblongata and of the frontopontine tract in the cerebral peduncle was assessed by loss of myelin, glial proliferation, and presence of macrophages, and indicated as + (present) or − (absent).

Results

Among six cases previously diagnosed as BIBD, neurofilament-positive inclusions were disclosed in two cases, and the inclusions also showed intense immunoreactivity to α-internexin; thus, the diagnosis of these cases was changed to NIFID. The other four cases were again diagnosed as BIBD. Limited clinical and pathological data in cases 1 [9], 2 [15], 3 [20], 5 [32, 36], and 6 [42] have been reported in Japanese.

Case reports

Case 1 (BIBD)

This man was 40 years old at the time of death. He initially complained of difficulty working in high places at age 34. Subsequently, weakness in the left hand and dysarthria developed. Neurological examination at age 35 revealed muscle weakness, fasciculation, and cerebellar ataxia including lack of coordination of the left side extremities. Apathy and oral dyskinesia also developed. Subsequently, involuntary movements such as an alien-hand sign to grasp something with the left hand, deviation of the tongue to the right side, and spastic paralysis in the left extremities also emerged. He obtained an IQ score of 89 on the Wechsler Adult Intelligence Scale (WAIS). At age 36, he could not walk without support. Reduction of utterance, impaired comprehension of speech, disorientation, bradykinesia, swallowing disturbance, ideomotor apraxia, and dressing apraxia were found. Weakness of the left facial muscles and four extremities, muscle atrophy of the tongue, left sternocleidomastoid muscle, and hands, and fasciculation of the legs were also observed. Deep tendon reflexes were hyperactive, and the Babinski sign was positive on the right side. Examinations of blood and cerebrospinal fluid were unremarkable. Electromyography and nerve conduction velocity testing were within normal limits, and neurogenic patterns were observed on muscle biopsy specimens. He died of pneumonia, with a clinical course of 6 years and 4 months. The final neurological diagnosis was amyotrophic lateral sclerosis (ALS) with dementia or Creutzfeldt-Jakob disease.

Case 2 (BIBD)

The patient was a man who was 63 years old at the time of death. He initially developed obsessive ideas and behaviors at the age of 57 years. Subsequently, stereotypic behaviors occurred. He had no relevant past medical or family history. Neurological examination at age 57 disclosed obsessive behaviors, impaired facial recognition, euphoria, and emotional incontinence. Baseline blood examinations were

within normal limits. He was tested using the WAIS and obtained an IQ score of 99. At age 58, apathy, restlessness, oral tendency, disorientation in time and place, impaired memory function, and disturbance of calculation ability were observed. No motor neuron signs, parkinsonism, or cerebellar symptoms were noted, and his gait was normal. He obtained an IQ score of 77 on the WAIS. Parkinsonism first developed at age 59 and primitive reflexes at age 63. He died about 6 years after the onset. The final neurological diagnosis was Pick's disease.

Case 3 (BIBD)

This was a housewife who was 67 years at the time of death. She presented initially with an obsession with collecting things at the age of 56. Subsequently, memory disturbance occurred. She neglected her housework and began to eat only rice and pickled vegetables. At age 58, she was inflexible, drinking too much, and had pica. She had no relevant past medical or family history. Neurological examination at age 58 revealed memory disturbance, impairment of calculation ability, disorientation, emotional unconcern, verbal perseveration, and lack of insight. Blood, urine, and cerebrospinal fluid examinations were within normal limits. Thereafter, double incontinence, verbal stereotypy, echolalia, and reduction of spontaneous speech output were found. She became bedridden at age 60. At age 65, involuntary movements like chorea of the head, four extremities, and trunk occurred. This was a quick, small movement, and she shook her head to the right or left side. In addition, athetosis-like movements of the left arm developed. She died of cardiac failure with a clinical course of 12 years. Her neurological diagnosis was Pick's disease.

Case 4 (BIBD)

This was a 47-year-old man at the time of death. His initial symptom was self-centered behavior at the age of 40; subsequently, disinhibition, irritability, and stereotypic behaviors also occurred. He had no relevant past medical or family history. Neurological examination at age 42 disclosed indifference and lack of insight. The snout reflex was positive. Memory disturbance, aphasia, and constructional impairment were not found. A verbal fluency test revealed poor generation of words (animals = 10, letters = 4). He scored 27/30 on the MMSE (cut off: 24/25) and 25/36 on Raven's Colored Progressive Matrices (cut-off: 24/25). On the WAIS-Revised (WAIS-R), he obtained a verbal IQ score of 77, performance IQ score of 68, and full-scale IQ score of 70. On the Wechsler Memory Scale-Revised (WMS-R, mean $\pm$ standard deviation in all subscales = 100 ± 15), he obtained scores on verbal memory of 64, visual memory of 57, general memory of 50, attention/concentration of 80, and delayed recall <50. Restlessness, irritability, and social breakdown became increasingly remarkable. Thereafter, bilateral forced grasping, rigidity in the four extremities, retrocollis, reduction of utterance, aspontaneity, and sexual disinhibition developed. He died of pneumonia with a clinical course of about 7 years. His neurological diagnosis was the frontal-predominant type of Pick's disease.

Case 5 (NIFID)

This was a 73-year-old woman at the time of death. She presented initially with difficulty speaking clearly at the age of 67 years. Thereafter, she was aware of writing incomprehensible sentences. She had no relevant past medical or family history. Neurological examination at age 68 disclosed dysarthria, forced laughing, and effortful and monotonous speech output. Palatal reflex and pharyngeal reflex were decreased. Muscle weakness, atrophy, fasciculation, or pathological reflex was not found. Deep tendon reflex was slightly increased in the four extremities. Upward gaze was slightly restricted. Buccofacial apraxia was found. Baseline blood, urine, and cerebrospinal fluid examinations were unremarkable. An electromyogram was within normal limits. Verbal IQ and performance IQ scores tested by the WAIS-R were 100 and 87, respectively, and a full-scale IQ score was 94. She scored 161/165 on the Token test. She showed poor results on the Wisconsin Card Sorting test, presumably because of an inability to shift attention and frontal dysfunction, attaining only one category with frequent perseverative errors. On the Western Aphasia Battery (WAB), she scored 8/10 for information content, 9.2/10 for auditory word recognition, 4.2/10 for repetition, 8.6/10 for object naming, 6/10 for word fluency, 9.8/10 for reading aloud, and 10/10 for spontaneous writing. Abilities of naming, aural comprehension, and reading were preserved. On the WMS-R, she scored 128 for verbal memory, 68 for visual memory, 84 for general memory, 80 for attention/concentration, and 74 for delayed memory. At age 69, swallowing disturbance, repetitive motor actions, and gait instability occurred, and her utterance was limited to moans. Thereafter, vertical supranuclear gaze palsy, bradykinesia, rigidity, anterocollis, forced grasping, bilateral Babinski signs, dressing apraxia, fasciculation of the tongue, and myoclonus in the left arm developed. She died of pneumonia with a clinical course of 5 years and 8 months. The neurological diagnosis was slowly progressive aphasia.

Case 6 (NIFID)

A 29-year-old forwarding agent became aware of his disinhibited and self-centered behaviors. He started borrowing

money, used illegal stimulants, and repeatedly caused traffic accidents. Stereotypic behaviors also occurred. He was admitted to a psychiatric hospital at age 33. He had no relevant past medical or family history. Neurological examination revealed reduction of speech output, indifference, repetitive behaviors, emotional incontinence, sucking reflex, and urinary and fecal incontinence. Baseline blood, urine, and cerebrospinal examinations were unremarkable. Electromyography was within normal limits. Although he was initially suspected to have schizophrenia, the diagnosis was changed to early onset Pick's disease. Thereafter, forced grasping, sucking reflex, snout reflex, palmomental reflex, Babinski reflex, pica, utilizing behavior, and hypersexuality also developed. No muscle weakness, muscle atrophy, or impairment of spatial function was found. Electromyography and nerve conduction velocity testing were within normal limits. At age 36, flexion in all four extremities, swallowing difficulty, and bilateral ankle clonus developed. Rigidity and tremor were not observed during the course. He died of pneumonia at age 37 about 8 years after the onset.

Summary of clinical features of BIBD and NIFID

The clinical features in all BIBD and NIFID cases are summarized in Table 1. The mean age at onset was 46.8 ± 11.6 years in BIBD cases and 48.0 ± 26.9 years in NIFID cases. The mean disease duration was 7.8 ± 2.8 years in BIBD cases and 6.9 ± 1.6 years in NIFID cases. BIBD and NIFID cases shared several clinical features besides frontal symptoms. The onset symptoms were frontal syndrome in three BIBD and one NIFID cases. Other onset symptoms included muscle weakness (one BIBD case), dysarthria (one BIBD and one NIFID cases), and memory impairment (one BIBD case). Dementia developed more than 1 year after the onset in one BIBD and one NIFID cases, but did not exhibit frontal syndrome at onset. Dysarthria, dysphasia, upper and lower motor neuron signs, gait disturbance, parkinsonism, and parietal symptoms were noted in both diseases during the course. Memory impairment and involuntary movements like alien-hand sign, athetosis, and chorea were found only in BIBD cases in our series.

Radiological findings in BIBD and NIFID

The BIBD (case 4) and NIFID cases (cases 5 and 6) that were examined radiologically consistently showed rapidly progressive severe atrophy in the frontotemporal lobe and caudate nucleus. A flattened caudate nucleus was observed by 1–5 years after the onset (Figs. 1, 2). In both NIFID cases, the frontal atrophy was accentuated in the convexity, and the temporal base was relatively preserved in the early course. Positron emission tomography (PET) of a NIFID case (case 5) disclosed left side-predominant hypometabolism in the perisylvian region as well as frontal lobes, being compatible with the findings of corticobasal degeneration (CBD; data not shown).

Neuronal loss in BIBD and NIFID

The distribution of cerebral atrophy in BIBD and NIFID cases is shown in Table 2. The distribution of frontotemporal atrophy in our BIBD cases varied from case to case (Fig. 3a, b). However, in the NIFID cases, the frontal convexity was prominently affected, and the temporal base was relatively preserved (Fig. 3d, e, f). Atrophy of the frontal convexity was accentuated in the posterior portion rather than the anterior portion in one NIFID case (case 5; Fig. 3d). Evident atrophy in the precentral gyrus was found in two BIBD (cases 3 and 4) and both NIFID cases (Fig. 3a, b, d, e). All BIBD and NIFID cases showed severe caudate atrophy with a concavity of the ventricular surface (Fig. 3c, f).

Microscopically, BIBD and NIFID cases had similar topographical distributions and severities of neuronal loss (Table 2). Severe neuronal loss in the frontal and/or temporal cortex was frequently found in both diseases, and subcortical gliosis with loss of the myelin in the frontal lobes was evident in all BIBD and NIFID cases. No ischemic change was noted in the white matter in the frontotemporal lobe in any BIBD and NIFID case. Astrocytosis in the primary motor cortex was found in one NIFID and all BIBD cases, and severe neuronal loss was encountered in one BIBD case and one NIFID case. The corticospinal tract was degenerated in three BIBD and both NIFID cases (Fig. 4a, c). Various degrees of frontopontine tract degeneration were also noted in all BIBD and NIFID cases in which the cerebral peduncle was examined (Fig. 4e, f). Neurons in the hypoglossal nuclei were spared in number in all BIBD and one NIFID cases, although astrocyte proliferation in this site was frequently noted in both diseases. In two cases, one BIBD and one NIFID, which clinically exhibited lower motor neuron signs and for which spinal cord tissues were available, evident gliosis was found in the anterior horns; however, the anterior horn cells in these cases were spared in number (Fig. 4b, d). In the basal ganglia in both diseases, the caudate nucleus was consistently affected by severe neuronal loss (Fig. 5a). Severe degeneration was frequently found in the putamen also (Fig. 5b). Further, some of the BIBD and NIFID cases showed severe degeneration in the thalamus and globus pallidus. In both BIBD and NIFID, the neurons in the nucleus basalis of Meynert were relatively spared in number despite the presence of evident glial proliferation. The substantia nigra was affected by severe neuronal loss in all of our subjects, except for one

Table 1 Clinical features of BIBD and NIFID

	BIBD			NIFID		
	Case 1	Case 2	Case 3	Case 4	Case 5	Case 6
Sex	Male	Male	Female	Male	Female	Male
Age at onset (years)	34	57	56	40	67	29
Duration (years)	6.3	6	12	7	5.7	8
Initial symptoms	Weakness in the left hand, dysarthria	Obsessive behaviors	Behavioral change memory impairment, altered eating habits	Disinhibition	Dysarthria	Disinhibition
Prominent features	Motor neuron disease	Dementia	Dementia	Dementia	Dysarthria, aphasia	Dementia
Clinical diagnosis	ALS with dementia	Pick's disease	Pick's disease	Pick's disease	Slowly progressive aphasia	Early-onset Pick's disease
Oculomotor abnormalities					+	
Dysarthria	+				+	
Dysphasia	+			+	+	
Primitive reflex[a]		+		+	+	+
Gait disturbance	+	+	+	+	+	+
Upper motor neuron signs	+				+	+
Lower motor neuron signs	+				+	
Parkinsonism	+	+		+	+	
Disinhibition				+		+
Apathy, indifference	+	+	+	+	+	+
Economy of effort[b]		+		+		+
Reduction of utterance	+	+		+		+
Stereotypy		+	+	+	+	+
Oral tendency		+				+
Hypersexuality				+		+
Altered dietary habits			+			+
Apraxia and other parietal signs	+	+			+	
Buccofacial apraxia					+	
Memory impairment		+	+			
Face recognition impairment		+	+			
Involuntary movements[c]	+		+			
Cerebellar signs	+					

[a] Palmomental reflex, grasp reflex, sucking reflex, and/or snout reflex

[b] Denkfaulheit

[c] Alien-hand sign (case 1), athetosis (case 3), or chorea (case 3)

BIBD case in which the degeneration was moderate (Fig. 5c). Moderate to severe neuronal loss in the insular and cingulate cortices, amygdala, ambient gyrus, subiculum, and parahippocampal gyrus was consistently found in both diseases. The hippocampal pyramidal neurons were strikingly reduced in number in three BIBD cases for which tissue was available, and one NIFID case also (Fig. 6a, b). Furthermore, marked reduction of the hippocampal granular cells was encountered in two of the three BIBD cases for which tissue was available, and in one NIFID case (Fig. 6a, b).

Inclusion bodies in BIBD and NIFID

All BIBD and NIFID cases had a varying number of round or oval intraneuronal cytoplasmic inclusions (Fig. 7a, b, c). The two diseases could not be distinguished by the morphological features of the inclusions as revealed by conven-

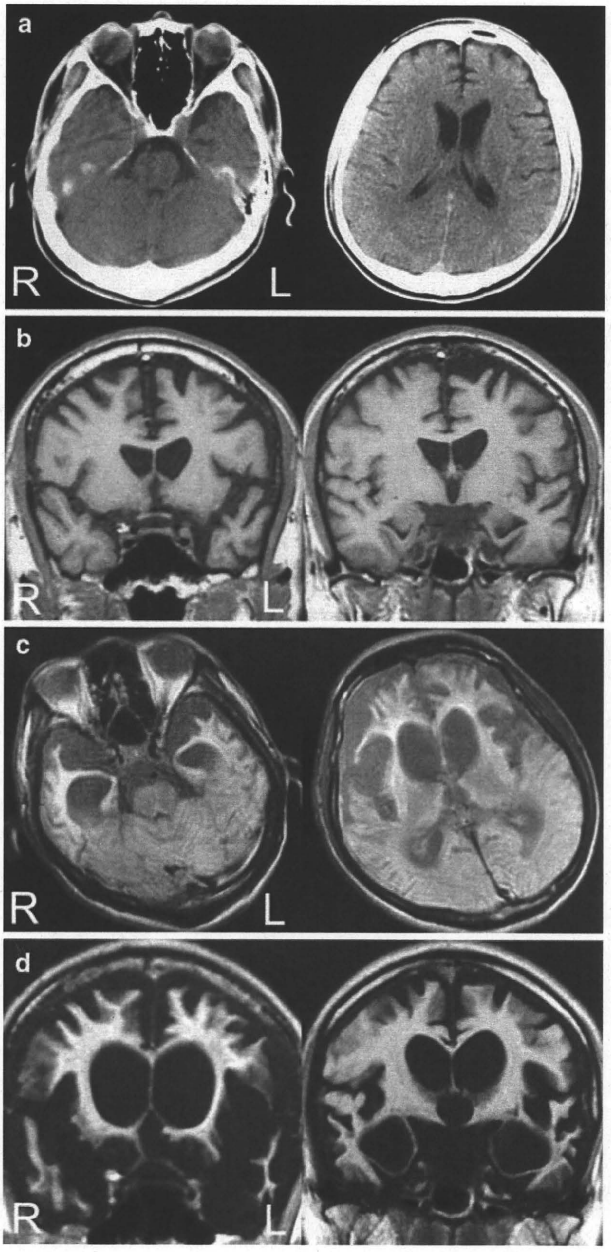

Fig. 1 Serial structural radiographic images of BIBD (case 4). Mild, but not negligible, atrophy in the frontal and temporal lobes and caudate nucleus is seen 2 years after the onset (**a**, **b**). The cortical atrophy is prominent in the frontal convexity and left superior temporal gyrus, and the temporal base is well spared at this time (**b**). Fluid attenuated inversion recovery (FLAIR) images 4 years after onset show severe atrophy in the basal ganglia including the caudate nucleus, frontal convexity, and temporal lobes (**c**, **d**)

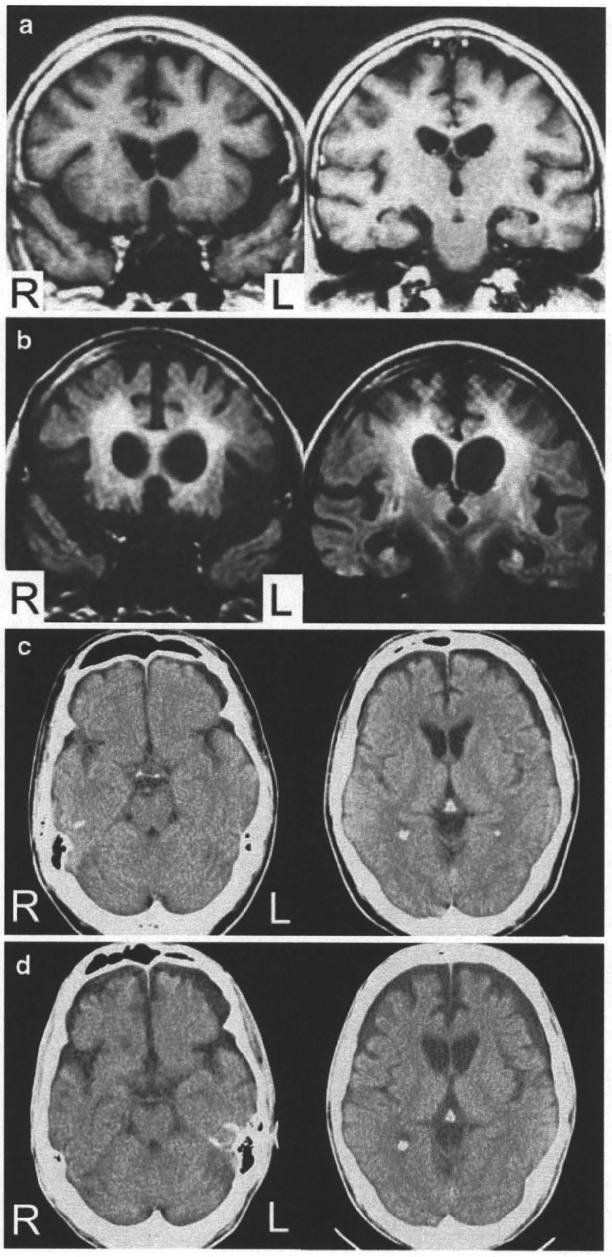

Fig. 2 Serial structural images of NIFID (cases 5 and 6). Coronal T1 images 16 months after the onset in case 5 clearly show the atrophy in the caudate nucleus (**a**). Five years after the onset, the severity of the frontal convexity in case 5 was more prominent in the posterior than in the anterior portion, and the temporal base appears to be spared (**b**). Serial CT images of NIFID in case 6 show mild atrophy in the frontal lobes and caudate nucleus 4 years after onset (**c**). The caudate nucleus is already flattened 5 years after onset, but the temporal lobes are relatively spared (**d**)

tional stains; however, intraneuronal cytoplasmic inclusions having distinct eosinophilic cores were noted only in one NIFID case (case 5, Fig. 7d).

In both NIFID cases, neurofilament-positive inclusions and α-internexin-positive inclusions were encountered in the affected cortex (Fig. 7e). Accumulations of neurofilaments as well as of α-internexin were seen in the hippocampal pyramidal neurons. These accumulations usually had a round or cap-like appearance. In contrast to these aggregates, the spherical inclusions with distinct eosinophilic cores observed in one NIFID case (case 5) were α-internexin-negative and neurofilament-negative (Fig. 7f, g, i, j). Inclusions with cores were frequently encountered in the CA3-4 of the hippocampus and pontine nucleus.

Table 2 Distribution of pathological changes in BIBD and NIFID

	BIBD				NIFID	
	Case 1	Case 2	Case 3	Case 4	Case 5	Case 6
Brain weight (g)	1,230	1,140	880	940	940	940
Cerebral atrophy	Ttip	Ftip, Fbase, Tbase	Ftip, Fbase, Tbase	F, Tbase	Fconv	Fconv, Ttip
Neuronal loss and astrocytosis						
Superior frontal gyrus	+++	+++	++	+++	+++	++
Medial frontal gyrus	+++	+	++	+++	++	+
Inferior frontal gyrus	+++	++	++	+++	++	+
Orbital gyrus	+++	+++	+	+++	+	++
Primary motor cortex	+++	+	+	+[a]	+++[a]	−[a]
Superior temporal gyrus	+++	+	++	+++	+	++
Medial temporal gyrus	+++	++	+++	+++	++	+
Inferior temporal gyrus	+++	+++	+++	+++	++	−
Parietal cortex	+	na	na	+	++	−
Insular cortex	+++	++	+++	+++	+++	++
Cingulate gyrus	+++	+++	+++	+++	++	++
Amygdala	+++	+++	na	+++	+++	++
Ambient gyrus	+++	++	+++	+++	+++	++
CA1 of hippocampus	+++	+++	+++	na	+++	−
Hippocampal dentate gyrus	+++	++	+++	na	++	−
Subiculum	+++	+++	+++	na	+++	+++
Entorhinal cortex	+++	+++	na	na	++	++
Parahippocampal gyrus	+++	++	+++	+++	++	++
Caudate nucleus	+++	+++	+++	+++	+++	+++
Putamen	+++	++	+++	+++	+++	+++
Globus pallidus	++	++	++	++	+++	++
Thalamus	+	++	±	+++	+++	+
Subthalamic nucleus	±	±	na	±	na	±
Nucleus basalis of Meynert	+	±	±	±	±	±
Dentate nucleus of	+	±	±	±	±	−
Cerebellum						
Trochlear nucleus	na	±	na	±	±	±
Oculomotor nucleus	na	na	na	na	±	±
Substantia nigra	+++	++	+++	+++	+++	+++
Red nucleus	±	na	±	na	±	±
Locus ceruleus	++	±	±	++	±	+
Pontine nucleus	±	±	±	±	±	±
Dorsal vagal nucleus	±	na	±	±	±	−
Hypoglossal nucleus	±	±	±	±	+	±
Inferior olivary nucleus	+	±	±	+	++	±
Frontopontine tract	na	+[b]	+[b]	+[b]	+	+
Corticospinal tract						
Cerebral peduncle	na	−	+	+	+[c]	+
Medulla oblongata	+	−	+	+	+	+
Anterior horn	±	na	na	na	±	na

F frontal, *Ftip* Frontal tip, *Fbase* frontal base, *Fconv* frontal convexity, *Ttip* temporal tip, *Tbase* temporal base. The severity of degeneration in the cerebral cortex, basal ganglia, and brainstem nuclei: -, no histopathological alteration; ± , no neuronal loss but gliosis; +, slight neuronal loss and gliosis; ++, moderate neuronal loss and gliosis; +++, severe neuronal loss and gliosis. Degeneration in the pyramidal tract and that in the frontopontine tract: +, present; –, absent. See details in the text. *na* not available

[a] Moderate astrocytosis was found in the deep cortical layer and adjacent white matter

[b] Degeneration was more evident in the frontopontine tract than in the corticospinal tract at the level of the cerebral peduncle

[c] Degeneration was more evident in the corticospinal tract than in the frontopontine tract at the level of the cerebral peduncle

Because the inclusions with cores were hematoxylin-positive, they were readily distinguished from α-internexin and neurofilament aggregates even in the single immunohistochemistry. Some of the inclusions with cores were surrounded by various amounts of α-internexin and neurofilament aggregates, ranging from a small accumulation (Fig. 7g) to

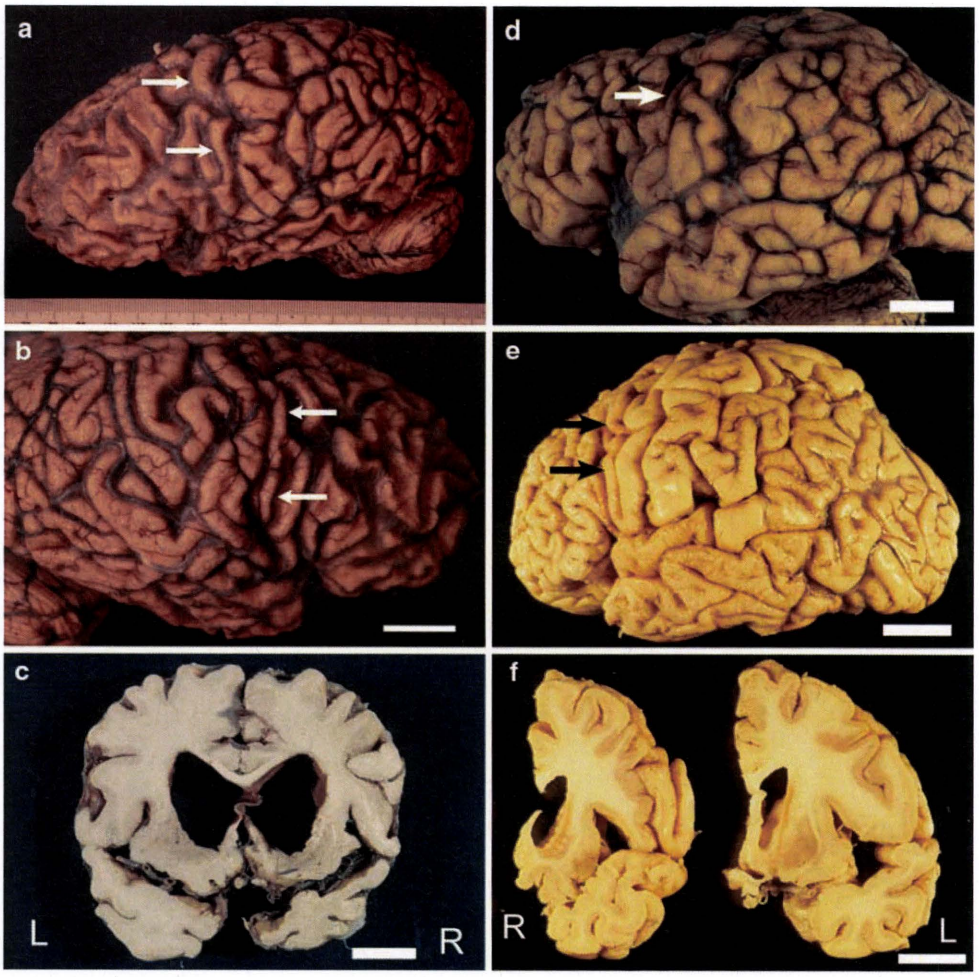

Fig. 3 Macroscopic findings in BIBD and NIFID. **a**, **b** Marked atrophy of the frontal and temporal lobes in BIBD (case 3). The bilateral precentral gyri are atrophic (*arrows*). **c** Severe atrophy in the basal ganglia as well as the right temporal lobe in BIBD (case 2). Severe dilation of the lateral ventricles with concavities of the ventricular surface is seen. **d** Severe atrophy in the frontal convexity in NIFID (case 5). The most severely affected region appears to be the precentral gyrus (*arrow*). The temporal cortices appear to be spared. **e** Severe atrophy in the frontal cortices including the precentral gyrus (*arrows*) in NIFID (case 6). **f** Although caudate atrophy is prominent, the frontotemporal cortices appear to be relatively spared in NIFID (case 6). All scale bars = 2 cm

a dense and diffuse cytoplasmic pattern (Fig. 7h). In a few of the inclusions with cores that were surrounded by dense aggregates of α-internexin or neurofilament, weak to intense immunoreactivity of α-internexin or neurofilament, respectively, was noted. The inclusions with cores usually contained the epitope of p62 (Fig. 7k). Some of the inclusions with cores also showed weak ubiquitin immunoreactivity. In both NIFID cases, there were no lesions immunostained by anti-C-terminal-specific p62, TDP-43, or polyglutamine antibody. Double immunohistochemistry demonstrated that p62-positive spherical inclusions with cores frequently coexisted with α-internexin-positive inclusions in the cytoplasm of the hippocampal pyramidal neurons (Fig. 7l, m, n, o, p, q). The cores of the inclusions showed absent or only weak p62 immunoreactivity (Fig. 7l, m, n, o, p). α-Internexin aggregates often showed spicules or a tangle-like appearance (Fig. 7p, q). Both p62 and α-internexin aggregates were also found in the cytoplasm of the dentate granular cells, which were often intermingled (Fig. 7r). Although no inclusions with cores were seen in the other NIFID case, a small number of p62-positive inclusions were found in the hippocampus and pontine nucleus. No intranuclear inclusions immunopositive for neurofilament, α-internexin, or p62 were found in our NIFID cases.

In the BIBD cases, no immunoreactivity of tau, α-synuclein, ubiquitin, neurofilament, α-internexin, TDP-43, polyglutamine, or p62-C was seen in inclusions. However, some inclusions in the pontine nucleus in cases 1, 2, and 4 were labeled with anti-N-terminus of p62 antibody (Fig. 7s).

The distribution of basophilic inclusion bodies in BIBD cases was consistent with that reported previously [24]: the inclusions were most frequently found in the basal ganglia and brainstem nuclei. The inclusions were also found in the motor neurons in the hypoglossal nuclei in three BIBD cases (cases 1, 3, and 4) and in the spinal anterior horn cells in one BIBD case (case 1), who presented clinically with lower motor neuron signs. Although scant, the inclusions were noted in the hippocampus, subiculum, parahippocampal gyrus, amygdala, and cerebellar dentate nucleus. In NIFID cases, α-internexin-positive inclusions were frequently observed in the frontotemporal cortex, hippocampal pyramidal neurons, and dentate granular cells. Many inclusions were also encountered in the pontine nucleus (cases 5 and 6) and inferior olivary nucleus (case 5), and to

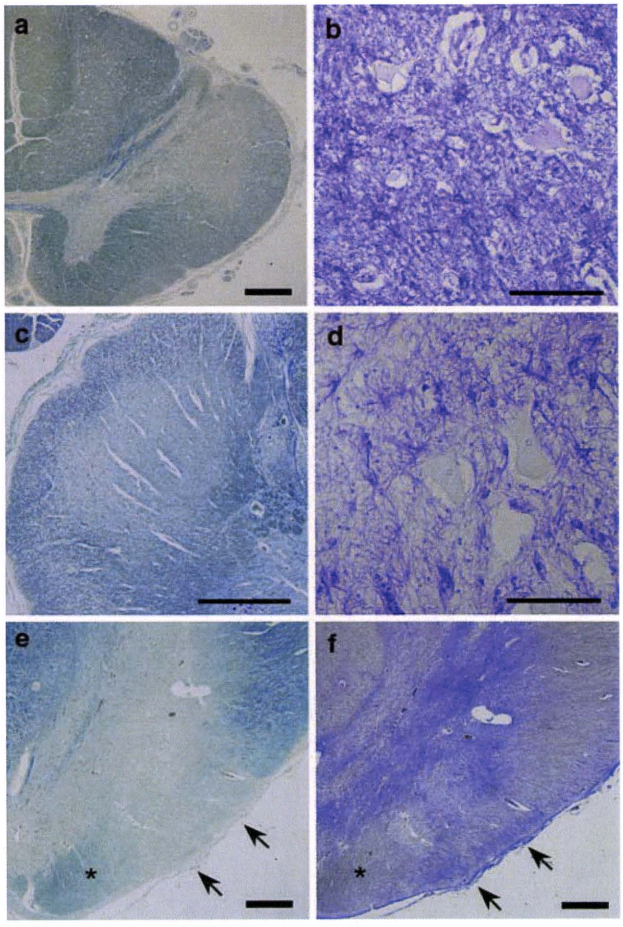

Fig. 4 Motor system involvement in BIBD and NIFID. **a** The cervical cord in BIBD (case 1). Evident loss of myelin in the corticospinal tract is seen. **b** The cervical cord in BIBD (case 1). Severe gliosis in the anterior horn is noted, although the anterior horn cells appear to be spared in number. **c** The cervical cord in NIFID (case 5). Severe loss of myelin in the corticospinal tract is observed. **d** The lumbar cord in NIFID (case 5). Evident gliosis in the anterior horn is seen, but neurons are spared. **e**, **f** Evident loss of myelin with gliosis in the corticospinal tract in the cerebral peduncle (*arrows*) in an NIFID case (case 5). The corticobulbar fibers appear to be involved also, but the degeneration in the frontopontine tract is relatively mild in this case (*asterisks*). **a**, **c**, **e** KB stain; **b**, **d**, **f** Holzer stain. Scale bars = (**a**, **c**, **e**, **f**) 1 mm, (**b**, **d**) 100 μm

a lesser frequency, in the dentate nucleus in the cerebellum (case 5).

None of the cases showed neurofibrillary changes, argyrophilic grains, senile plaques, Lewy bodies, or Pick bodies on silver-stained or immunostained sections. No immunoreactivity of TDP-43 was noted in the spinal cord, hypoglossal nuclei, hippocampus, or frontotemporal cortices in BIBD and NIFID cases.

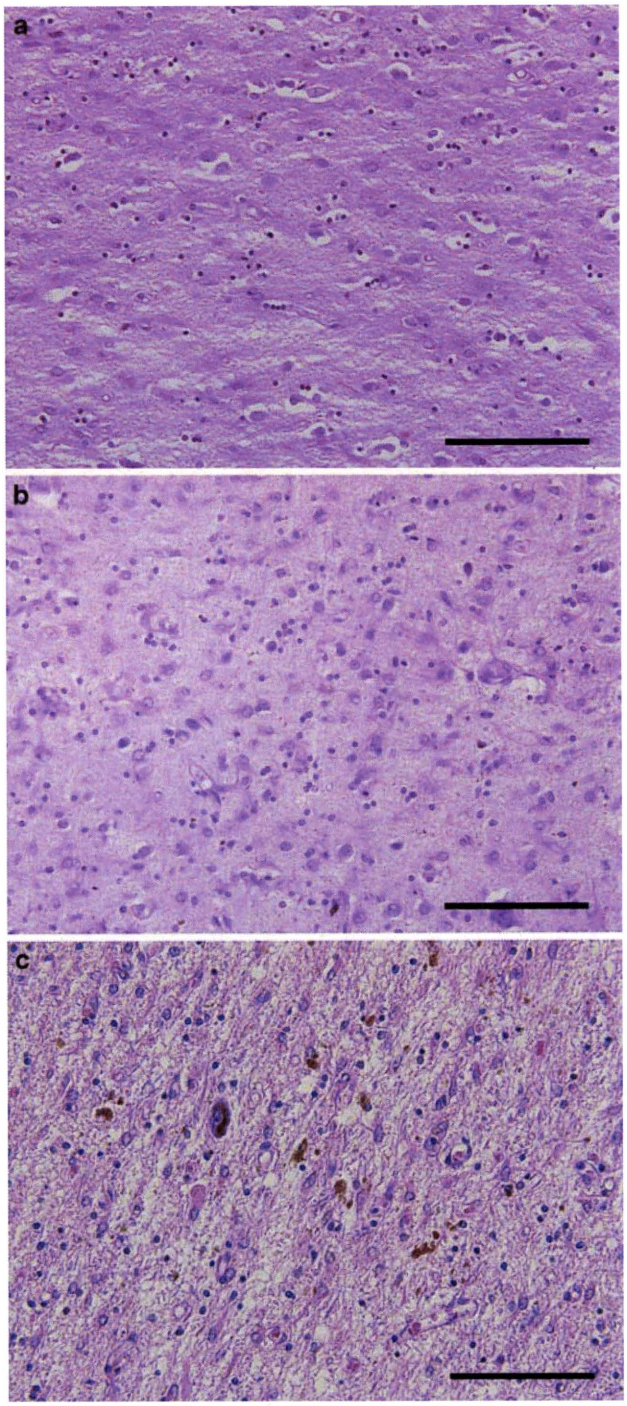

Fig. 5 The basal ganglia and substantia nigra in BIBD and NIFID. **a** Marked neuronal loss and astrocytosis with tissue rarefaction in the caudate nucleus in a BIBD case (case 2). **b** Severe neuronal loss with astrocytosis in the putamen in a BIBD case (case 3). **c** Severe neruonal loss and astrocytosis in the substantia nigra in a NIFID case (case 6). Free melanin was also scattered. **a**, **b**, **c** H&E stain. All scale bars = 100 μm

Discussion

Among six cases previously diagnosed as having basophilic inclusions using conventional stains, the diagnosis of two cases (33%) was changed to NIFID. The clinical features of our NIFID cases were consistent with those reported previously. NIFID cases and BIBD cases shared several clinical

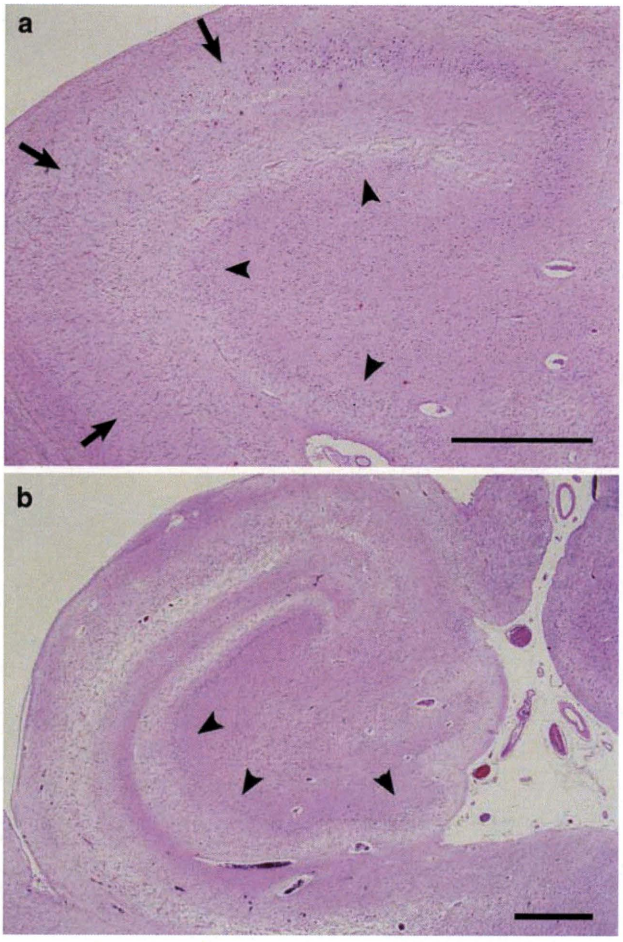

Fig. 6 Severe degeneration of the hippocampus in BIBD and NIFID. **a** BIBD (case 2). *Arrows* indicate severe loss of pyramidal neurons from the CA1 to the subiculum. In addition, the dentate granular cells have almost completely disappeared (*arrowheads*). **b** NIFID (case 5). The pyramidal neurons from the subiculum to CA4 have almost completely disappeared. The dentate granular cells are evidently reduced in number (*arrowheads*). **a**, **b** H&E stain. Scale bars = (**a**, **b**) 1 mm

features besides frontal symptoms, including dysarthria, motor neuron signs, parkinsonism, memory impairment, and parietal symptoms. Given these findings, it seemed to be difficult to clinically differentiate NIFID from BIBD. The distribution and severity of neuronal loss in BIBD cases also resembled those in NIFID cases: severe degeneration was frequently found in the caudate nucleus, putamen, substantia nigra, and pyramidal tract, as well as the frontotemporal cortex. Severe neuronal loss in the hippocampal pyramidal neurons was noted in all three BIBD cases for which the tissues were available and one NIFID case. Further, all of these cases had moderate to severe loss of the granular cells in the hippocampal dentate gyrus. The distribution corresponded to the clinical manifestations of both diseases.

In our BIBD and NIFID cases, the precentral gyrus and pyramidal tract were frequently affected, while the lower motor neurons tended to be spared in number. In previous BIBD cases, especially in MND cases with basophilic inclusions, clinical and pathological evidence of both upper and lower motor neuron involvement was often described. In previous NIFID cases also, the pyramidal tract degeneration was frequently noted, while the lower motor neuron degeneration in NIFID was frequently minimal [7, 17]. Although it is unusual, some of our BIBD and NIFID cases presented clinically with lower motor neuron signs, but did not have significant neuronal loss in the spinal anterior horn cells. The development of lower motor neuron signs in these cases may be explained by the formation of neuronal inclusions with evident astrocytosis in the corresponding sites. Although weakness was noted in some of the previous NIFID cases [7, 17], as far as we know, other lower motor neuron signs including fasciculation and muscle atrophy are rare in NIFID [4, 17, 21, 31]. These clinical findings also appear to support the view that the motor system involvement in NIFID tends to be restricted to the precentral gyrus and pyramidal tract. Further pathological findings need to be accumulated to clarify the histopathological profiles of motor system involvement in BIBD and NIFID.

TDP-43 accumulation is observed in several diseases with motor system involvement, including amyotrophic lateral sclerosis (ALS), FTLD with ubiquitin pathology (FTLD-U) [3, 29], Guamanian parkinsonism–dementia complex (PDC) [12], and Guamanian ALS [10], and to a lesser degree, in some diseases without motor neuron degeneration [2, 26]. In our BIBD and NIFID cases, TDP-43 immunoreactivity was not found in any inclusions, motor neurons, the hippocampal dentate gyrus, or the frontotemporal cortex, which are the preferred sites of TDP-43 accumulation in ALS and FTLD-U. In the consensus criteria recently reported by the Consortium for FTLD also [8], it was accepted that BIBD cases usually lack TDP-43 accumulation, although some of the neurons bearing basophilic inclusions in BIBD cases can show fine granular perikaryal immunoreactivity of TDP-43. Our results also support the view that TDP-43 is not a major pathogenic protein in BIBD and NIFID.

It is noteworthy that the cerebral atrophy in the NIFID cases was accentuated in the frontal convexity rather than the temporal base. Further, in one NIFID case, the frontal atrophy was more prominent in the posterior portion and extended to the parietal region. These findings are in accordance with the previous view that the parietal cortex in NIFID is often affected [7, 17], and that NIFID cases can exhibit CBD-like symptoms including apraxia [16, 17]. On the other hand, alien-hand sign and apraxia were also observed in our BIBD cases, suggesting that BIBD as well as NIFID should be included in the differential diagnosis of a patient presenting with CBD-like symptoms.

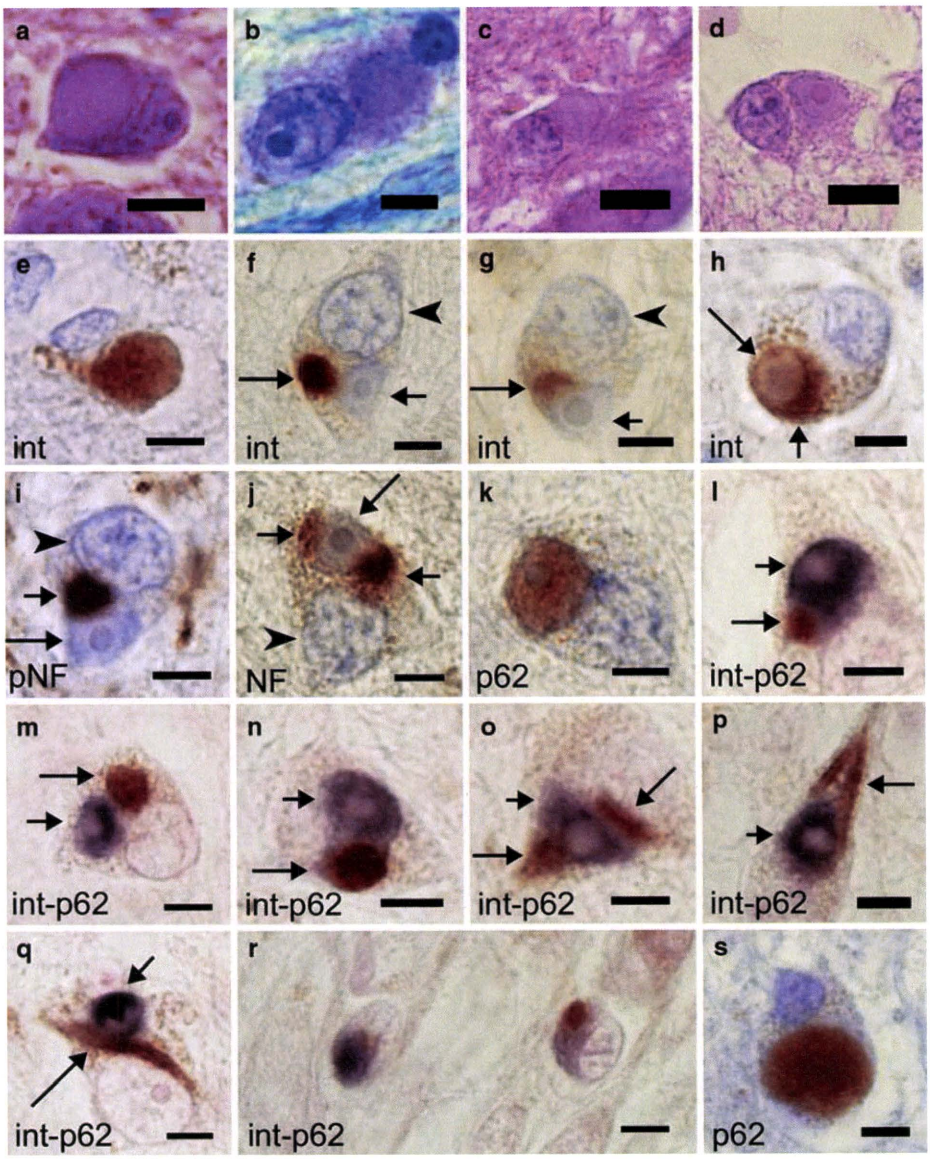

Fig. 7 Intraneuronal inclusions in BIBD (**a**, **b**, **s**) and NIFID (**c**, **d**, **e**, **f**, **g**, **h**, **i**, **j**, **k**, **l**, **m**, **n**, **o**, **p**, **q**, **r**). **a** An inclusion in the pontine nucleus in BIBD. **b** An inclusion in the nucleus basalis of Meynert in BIBD. **c** An inclusion without an eosinophilic core in the pontine nucleus in NIFID. **d** An inclusion with a distinct eosinophilic core (so-called cherry spot) in the CA4 in NIFID. **e** An α-internexin-positive inclusion in the frontal cortex in NIFID. **f** An α-internexin-positive inclusion in a hippocampal pyramidal neuron in NIFID (*long arrow*). The neuron also has an α-internexin-negative inclusion with a distinct core, which appears to correspond to the so-called cherry spot (*short arrow*). An *arrowhead* indicates a nucleus. **g** α-Internexin-negative inclusions with cores in NIFID (*short arrow*) were often accompanied by various amounts of α-internexin accumulation (*long arrow*). An *arrowhead* indicates a nucleus. The CA4. **h** Inclusions with cores in NIFID (*long arrow*) were often surrounded by a dense and diffuse cytoplasmic accumulation of α-internexin (*short arrow*). The pontine nucleus. **i**, **j** Most of the inclusions with cores in NIFID (*long arrows*) were hardly recognized by anti-neurofilament antibodies. *Short arrows* indicate neurofilament aggregates that contact the inclusions with cores. *Arrowheads* indicate nuclei. The CA4. **k** Inclusions with cores in NIFID usually show intense p62immunoreactivity. The CA4. **l**, **m**, **n**, **o** Inclusions with cores in NIFID were p62-positive, but the cores themselves were p62-negative (*black, short arrows*). α-Internexin aggregates frequently coexisted with the p62-positive inclusions with cores in the same neuron (*brown, long arrows*). The hippocampal CA4. **p** Two spicule-shaped neurofilament-positive inclusions (*brown, long arrow*) and a p62-positive spherical inclusion (*black, short arrow*) in a hippocampal neuron in NIFID. The core of the latter inclusion is p62-negative. **q** An α-internexin-positive inclusion showing a spicule-like appearance in NIFID (*brown, long arrow*). A p62-positive round inclusion with a hollow appearance is also present in the same neuron (*black, short arrow*). The CA3. **r** (α-Internexin (*brown*) and p62 (*black*) aggregates in the hippocampal dentate gyrus in NIFID. They were often intermingled. **s** Some inclusions in the pontine nucleus in BIBD cases are p62-positive. **a**, **c**, **d** H&E stain; **b** Klüver-Barrera stain; **e**, **f**, **g**, **h** (α-internexin immunohistochemistry. **i** SMI31 immunohistochemistry; **j** SMI32 immunohistochemistry; **k**, **s** p62-N immunohistochemistry; l, **m**, **n**, **o**, **p**, **q**, **r** double immunohistochemistry using anti-α-internexin antibody (*brown*) and anti-N-terminal specific p62 antibody (*black*). **a** Case 3; **e** case 6; **c**, **d**, **f**, **g**, **h**, **i**, **j**, **k**, **l**, **m**, **n**, **o**, **p**, **q**, **r** case 5; **b**, **s** case 2. Scale bar = (**a**, **b**, **c**, **d**) 10 μm, (**e**, **f**, **g**, **h**, **i**, **j**, **k**, **l**, **m**, **n**, **o**, **p**, **q**, **r**, **s**) 5 μm

The degeneration of the basal ganglia in the BIBD and NIFID cases, which did not differ between the two diseases, was more severe and extensive than that in CBD. In our previous semiquantitative study, the globus pallidus and substantia nigra in CBD cases usually showed severe degeneration with fibrous gliosis, but unlike BIBD and NIFID, the putamen and caudate nucleus did not [38]. The development of involuntary movements observed in our BIBD cases might be associated with the severe alteration in the striatum.

All of our BIBD cases for which the tissue was available had severe neuronal loss with gliosis in the hippocampus, although this site was originally reported to be spared in BIBD [24]. Further, all these cases also showed evident loss of dentate granular cells with severe astrocytosis. Loss of neurons in the hippocampus including the dentate gyrus was also observed in one NIFID case. As far as we know, although a varying degree of neuronal loss in the hippocampal pyramidal neurons in NIFID has been described, a reduction in the number of dentate granular cells has not been noted in any previous NIFID case [4, 7, 16, 21, 27]. Whether the severity of the hippocampal lesion differs in NIFID and BIBD remains to be elucidated.

The NIFID cases examined in this study had two types of intraneuronal cytoplasmic inclusions that were differentiated immunohistochemically: (1) neurofilament- and α-internexin-positive round, cap-like, or spicule-shaped inclusions lacking cores and (2) p62-positive but neurofilament- or α-internexin-negative spherical inclusions bearing distinct eosinophilic cores. The morphological features of the latter inclusions were quite similar to those of the "compound intraneuronal inclusion bodies" described by Schochet and Earle in 1970 [35]. At least three cases with compound intraneuronal inclusion bodies have been reported, and interestingly, they were young-onset dementia or MND, and often showed remarkable frontotemporal and caudate atrophy and pyramidal tract degeneration [11, 33, 35]. More recently, Josephs et al. [16] called the eosinophilic core a "cherry spot". Several previous studies demonstrated the morphological and immunohistochemical heterogeneity of inclusions in NIFID. Bigio et al. [4] noted three different morphologic types of intracytoplasmic inclusions in a NIFID case: Pick-like bodies, pleomorphic inclusions, and hyaline conglomerate-like inclusions. They noted that a small number of Pick-like bodies were faintly neurofilament-positive, but the latter two inclusions showed intense neurofilament immunoreactivity. Mackenzie and Feldman [21] described two types of inclusions in an NIFID case: Pick body-like inclusions and hyaline conglomerate inclusions. They described Pick body-like inclusions as round or oval, consistently ubiquitin-positive, rarely neurofilament-positive, and often surrounded by diffuse cytoplasmic immunoreactivity of the neurofilament. They also noted that the center of some hyaline conglomerate inclusions had small, round or elongated eosinophilic masses, but the inclusions appeared to be irregular, sometimes multilobulated, and neurofilament-positive. Thus, the characteristics of the inclusions were not in accordance with those of the inclusions with eosinophilic cores that we observed. Uchikado et al. [40] also noted the presence of α-internexin-negative inclusions in NIFID. Like our results, they observed p62-positive and α-internexin-positive inclusions within the same neuron. However, they noted that round, p62-positive inclusions often occupied a central core of larger α-internexin inclusions, being inconsistent with our results that inclusions with eosinophilic cores were α-internexin-negative. Uchikado et al. further demonstrated electron microscopically that inclusions in NIFID contain two types of components. Based on the presence of neurofilament-negative inclusions, Mackenzie and Feldman [21] speculated that whether NIFID is a single disease entity remains to be elucidated. Indeed, our results led us to speculate that an unknown protein besides neurofilament and α-internexin may play a pivotal pathogenic role at least in some NIFID cases, and possibly, neurofilaments and α-internexin accumulate secondarily in NIFID cases having inclusions with eosinophilic cores. To understand the histopathological heterogeneity in NIFID, further immunohistochemical and biochemical findings need to be accumulated.

Acknowledgments We would like to thank Ms. H. Kondo (Department of Neuropathology, Tokyo Institute of Psychiatry), Ms. M. Onbe (Department of Neuropsychiatry, Okayama University Graduate School of Medicine, Dentistry and Pharmaceutical Sciences), Mr. T. Yoshimura (Kinoko Espoir Hospital), and Mr. Y. Shoda and Ms. K. Suzuki (Tokyo Institute of Psychiatry) for their excellent technical assistance and Mr. A. Sasaki for help with the production of the manuscript. This work was supported by a grant-in-aid for scientific research from the Ministry of Education, Culture, Sports, Science and Technology (14570957) and a research grant from the Zikei Institute of Psychiatry.

References

1. Aizawa H, Kimura T, Hashimoto K, Yahara O, Okamoto K, Kikuchi K (2000) Basophilic cytoplasmic inclusions in a case of sporadic juvenile amyotrophic lateral sclerosis. J Neurol Sci 176:109–113
2. Amador-Ortiz C, Lin WL, Ahmed Z, Personett D, Davies P, Duara R, Graff-Radford NR, Hutton ML, Dickson DW (2007) TDP-43 immunoreactivity in hippocampal sclerosis and Alzheimer's disease. Ann Neurol 61:435–445
3. Arai T, Hasegawa M, Akiyama H, Ikeda K, Nonaka T, Mori H, Mann D, Tsuchiya K, Yoshida M, Hashizume Y, Oda T (2006) TDP-43 is a component of ubiquitin-positive tau-negative inclusions in frontotemporal lobar degeneration and amyotrophic lateral sclerosis. Biochem Biophys Res Commun 351:602–611
4. Bigio EH, Lipton AM, White CL 3rd, Dickson DW, Hirano A (2003) Frontotemporal and motor neurone degeneration with neurofilament inclusion bodies: additional evidence for overlap between FTD and ALS. Neuropathol Appl Neurobiol 29:239–253

5. Cairns NJ, Perry RH, Jaros E, Burn D, McKeith IG, Lowe JS, Holton J, Rossor MN, Skullerud K, Duyckaerts C, Cruz-Sanchez FF, Lantos PL (2003) Patients with a novel neurofilamentopathy: dementia with neurofilament inclusions. Neurosci Lett 341:177–180
6. Cairns NJ, Zhukareva V, Uryu K, Zhang B, Bigio E, Mackenzie IR, Gearing M, Duyckaerts C, Yokoo H, Nakazato Y, Jaros E, Perry RH, Lee VM, Trojanowski JQ (2004) Alpha-internexin is present in the pathological inclusions of neuronal intermediate filament inclusion disease. Am J Pathol 164:2153–2161
7. Cairns NJ, Grossman M, Arnold SE, Burn DJ, Jaros E, Perry RH, Duyckaerts C, Stankoff B, Pillon B, Skullerud K, Cruz-Sanchez FF, Bigio EH, Mackenzie IR, Gearing M, Juncos JL, Glass JD, Yokoo H, Nakazato Y, Mosaheb S, Thorpe JR, Uryu K, Lee VM, Trojanowski JQ (2004) Clinical and neuropathologic variation in neuronal intermediate filament inclusion disease. Neurology 63:1376–1384
8. Cairns NJ, Bigio EH, Mackenzie IR, Neumann M, Lee VM, Hatanpaa KJ, White CL 3rd, Schneider JA, Grinberg LT, Halliday G, Duyckaerts C, Lowe JS, Holm IE, Tolnay M, Okamoto K, Yokoo H, Murayama S, Woulfe J, Munoz DG, Dickson DW, Ince PG, Trojanowski JQ, Mann DM. Consortium for Frontotemporal Lobar Degeneration (2007) Neuropathologic diagnostic and nosologic criteria for frontotemporal lobar degeneration: consensus of the Consortium for Frontotemporal Lobar Degeneration. Acta Neuropathol (Berl) 114:5–22
9. Doubutsu M, Hanyu S, Yosida M, Oyanagi S (1993) Immunohistochemical and ultrastructural investigation of argyrophilic neuronal cytoplasmic inclusions in a patient with ALS-like symptoms, dementia, cerebellar ataxia and extrapyramidal symptoms (in Japanese with English abstract). Neuropathology 13:31–38
10. Geser F, Winton MJ, Kwong LK, Xu Y, Xie SX, Igaz LM, Garruto RM, Perl DP, Galasko D, Lee VM, Trojanowski JQ (2007) Pathological TDP-43 in parkinsonism–dementia complex and amyotrophic lateral sclerosis of Guam. Acta Neuropathol (Berl) 115:133–145
11. Hamada K, Fukazawa T, Yanagihara T, Yoshida K, Hamada T, Yoshimura N, Tashiro K (1995) Dementia with ALS features and diffuse Pick body-like inclusions (atypical Pick's disease?). Clin Neuropathol 14:1–6
12. Hasegawa M, Arai T, Akiyama H, Nonaka T, Mori H, Hashimoto T, Yamazaki M, Oyanagi K (2007) TDP-43 is deposited in the Guam parkinsonism–dementia complex brains. Brain 130:1386–1394
13. Hilton DA, McLean B (2002) Case 291: rapidly progressive motor weakness, starting in pregnancy. Brain Pathol 12:267–268
14. Ishihara K, Araki S, Ihori N, Shiota J, Kawamura M, Nakano I (2006) An autopsy case of frontotemporal dementia with severe dysarthria and motor neuron disease showing numerous basophilic inclusions. Neuropathology 26:447–454
15. Ishino H, Yokoyama S, Nakashima Y, Otsuki S, Morisada A (1971) Atrophy of basal ganglia in Pick's disease (in Japanese with English abstract). Kyushu Neuropsychiatry 17:67–73
16. Josephs KA, Holton JL, Rossor MN, Braendgaard H, Ozawa T, Fox NC, Petersen RC, Pearl GS, Ganguly M, Rosa P, Laursen H, Parisi JE, Waldemar G, Quinn NP, Dickson DW, Revesz T (2003) Neurofilament inclusion body disease: a new proteinopathy? Brain 126:2291–2303
17. Josephs KA, Uchikado H, McComb RD, Bashir R, Wszolek Z, Swanson J, Matsumoto J, Shaw G, Dickson DW (2005) Extending the clinicopathological spectrum of neurofilament inclusion disease. Acta Neuropathol (Berl) 109:427–432
18. Kusaka H, Matsumoto S, Imai T (1990) An adult-onset case of sporadic motor neuron disease with basophilic inclusions. Acta Neuropathol (Berl) 80:660–605
19. Kusaka H, Matsumoto S, Imai T (1993) Adult-onset motor neuron disease with basophilic intraneuronal inclusion bodies. Clin Neuropathol 12:215–218
20. Kuyama K, Kuroda S, Morioka E, Oda T (1987) Pick's disease with argyrophilic inclusions in the basal ganglia and brainstem (in Japanese with English abstract). Neuropathology 8:35–44
21. Mackenzie IR, Feldman H (2004) Neurofilament inclusion body disease with early onset frontotemporal dementia and primary lateral sclerosis. Clin Neuropathol 23:183–193
22. Matsumoto S, Kusaka H, Murakami N, Hashizume Y, Okazaki H, Hirano A (1992) Basophilic inclusions in sporadic juvenile amyotrophic lateral sclerosis: an immunocytochemical and ultrastructural study. Acta Neuropathol (Berl) 83:579–583
23. Mizutani T, Sakamaki S, Tsuchiya N, Kamei S, Kohzu H, Horiuchi R, Ida M, Shiozawa R, Takasu T (1992) Amyotrophic lateral sclerosis with ophthalmoplegia and multisystem degeneration in patients on long-term use of respirators. Acta Neuropathol (Berl) 84:372–377
24. Munoz-Garcia D, Ludwin SK (1984) Classic and generalized variants of Pick's disease: a clinicopathological, ultrastructural, and immunocytochemical comparative study. Ann Neurol 16:467–440
25. Munoz DG (1998) The pathology of Pick complex. In: Kertesz A, Munoz DG (eds) Pick's Disease and Pick complex. Wiley-Liss, New York, pp. 211–241
26. Nakashima-Yasuda H, Uryu K, Robinson J, Xie SX, Hurtig H, Duda JE, Arnold SE, Siderowf A, Grossman M, Leverenz JB, Woltjer R, Lopez OL, Hamilton R, Tsuang DW, Galasko D, Masliah E, Kaye J, Clark CM, Montine TJ, Lee VM, Trojanowski JQ (2007) Co-morbidity of TDP-43 proteinopathy in Lewy body related diseases. Acta Neuropathol (Berl) 114:221–229
27. Nakazato Y, Ishida Y, Hoshi S, Amano Y (1985) Juvenile dementia with several types of neuronal inclusions (in Japanese with English abstract). Neuropathology 6:19–32
28. Nelson JS, Prensky AL. Sporadic juvenile amyotrophic lateral sclerosis (1972) A clinicopathological study of a case with neuronal cytoplasmic inclusions containing RNA. Arch Neurol 27:300–306
29. Neumann M, Sampathu DM, Kwong LK, Truax AC, Micsenyi MC, Chou TT, Bruce J, Schuck T, Grossman M, Clark CM, McCluskey LF, Miller BL, Masliah E, Mackenzie IR, Feldman H, Feiden W, Kretzschmar HA, Trojanowski JQ, Lee VM (2006) Ubiquitinated TDP-43 in frontotemporal lobar degeneration and amyotrophic lateral sclerosis. Science 314:130–133
30. Oda M, Akagawa N, Tabuchi Y, Tanabe H (1978) A sporadic juvenile case of the amyotrophic lateral sclerosis with neuronal intracytoplasmic inclusions. Acta Neuropathol (Berl) 44:211–216
31. Roeber S, Bazner H, Hennerici M, Porstmann R, Kretzschmar HA (2006) Neurodegeneration with features of NIFID and ALS—extended clinical and neuropathological spectrum. Brain Pathol 16:228–234
32. Sakajiri K, Bandou M, Yamanouchi H, Ishii K, Fukusako Y (1992) Slowly progressive dysarthria and impaired language function—a case report (in Japanese). Rinsho Shinkeigaku 32:1107–1111
33. Sam M, Gutmann L, Schochet SS Jr, Doshi H (1991) Pick's disease: a case clinically resembling amyotrophic lateral sclerosis. Neurology 41:1831–1833
34. Sasaki S, Toi S, Shirata A, Yamane K, Sakuma H, Iwata M (2001) Immunohistochemical and ultrastructural study of basophilic inclusions in adult-onset motor neuron disease. Acta Neuropathol (Berl) 102:200–206
35. Schochet SS Jr, Earle KM (1970) Pick's disease with compound intraneuronal inclusion bodies. Acta Neuropathol (Berl) 15:293–297
36. Tsuchiya K, Ishizu H, Nakano I, Kita Y, Sawabe M, Haga C, Kuyama K, Nishinaka T, Oyanagi K, Ikeda K, Kuroda S (2001) Distribution of basal ganglia lesions in generalized variant of Pick's disease: a clinicopathological study of four autopsy cases. Acta Neuropathol (Berl) 102:441–448

37. Tsuchiya K, Matsunaga T, Aoki M, Haga C, Ooe K, Abe K, Ikeda K, Nakano I (2001) Familial amyotrophic lateral sclerosis with posterior column degeneration and basophilic inclusion bodies: a clinical, genetic and pathological study. Clin Neuropathol 20:53–59
38. Tsuchiya K, Ikeda K (2002) Basal ganglia lesions in 'Pick complex: a topographic neuropathological study of 19 autopsy cases. Neuropathology 22:323–336
39. Uchikado H, Shaw G, Wang DS, Dickson DW (2005) Screening of neurofilament inclusion disease using α-internexin immunohistochemistry. Neurology 64:1658–1659
40. Uchikado H, Li A, Lin WL, Dickson DW (2006) Heterogeneous inclusions in neurofilament inclusion disease. Neuropathology 26:417–421
41. Wohlfart G, Swank RL (1941) Pathology of amyotrophic lateral sclerosis. Fiber analysis of the ventral roots and pyramidal tracts of the spinal cord. Arch Neurol Psychiatr 46:783–799
42. Yamasue H, Tsuchiya K, Kuroki N, Honada M, Niizato K, Anno M, Ikeda K, Kazamatsuri H (2000) A clinical case of sporadic frontal Pick's disease with onset at 29 years old of age (in Japanese with English abstract). Seishin Igaku (Clin Psychiatr) 42:1271–1277
43. Yokota O, Tsuchiya K, Oda T, Ishihara T, de Silva R, Lees AJ, Arai T, Uchihara T, Ishizu H, Kuroda S, Akiyama H (2006) Amyotrophic lateral sclerosis with dementia: an autopsy case showing many Bunina bodies, tau-positive neuronal and astrocytic plaque-like pathologies, and pallido-nigral degeneration. Acta Neuropathol (Berl) 112:633–645

CE: Satish ED: Prabhu Op: Jay WNR: LWW.WNR4299

NEUROREPORT

Presynaptic and postsynaptic nigrostriatal dopaminergic functions in multiple system atrophy

Masaya Hashimoto[a,c], Keiichi Kawasaki[a], Masahiko Suzuki[a,c], Kazuko Mitani[a,d], Shigeo Murayama[b], Masahiro Mishina[a,e], Keiichi Oda[a], Yuichi Kimura[a], Kiichi Ishiwata[a], Kenji Ishii[a] and Kiyoharu Inoue[c]

[a]Positron Medical Center, [b]Department of Neuropathology, Tokyo Metropolitan Institute of Gerontology, [c]Department of Neurology, Jikei University School of Medicine, [d]Department of Neurology, Tokyo Metropolitan Geriatric Hospital, Tokyo and [e]Neurological Institute, Nippon Medical School Chiba Hokusoh Hospital, Chiba, Japan

Correspondence to Kenji Ishii, Positron Medical Center, Tokyo Metropolitan Institute of Gerontology, 1-1 Naka-cho, Itabashi-ku, Tokyo 173-0022, Japan

Tel: +81 3 3964 3241 EX3503; fax: +81 3 3964 2188; e-mail: ishii@pet.tmig.or.jp

Received 7 September 2007; accepted 30 October 2007

A simultaneous evaluation of presynaptic and postsynaptic dopaminergic positron emission tomography markers, the dopamine transporters and the dopamine D_2-like receptors, was performed in eight patients with parkinsonian phenotype of multiple system atrophy. Both presynaptic and postsynaptic markers were revealed to have declined in such a manner that they kept strong positive correlation throughout the striatum of all patients, suggesting that the degeneration process in the striatum may involve the entire structure of the dopaminergic synapse. In two L-3,4,dihydroxyphenyl-alanine-responsive cases, the balance of decline in two markers was relatively shifted to presynaptic dominant side. Correlative positron emission tomography study of presynaptic and postsynaptic dopaminergic function may be useful for the diagnosis of multiple system atrophy and to understand the mechanisms of its temporal L-3,4,dihydroxyphenyl-alanine responsiveness. *NeuroReport* 00:000–000 © 2008 Wolters Kluwer Health | Lippincott Williams & Wilkins.

Keywords: dopamine receptor, dopamine transporter, L-3,4,dihydroxyphenyl-alanine responsiveness, multiple system atrophy, Parkinson, positron emission tomography

Introduction

In patients with the parkinsonian phenotype of multiple system atrophy (MSA-P), a pathological abnormality is observed mainly in the substantia nigra (SN), striatum, ceruleus nucleus, pontine nuclei, inferior olivary nucleus, cerebellum, and spinal cord. The impairment is particularly severe in the SN and striatum [1], and neuronal loss and gliosis are the features of the pathology [2]. Neuroimaging studies using positron emission tomography (PET) [3] and single photon emission computed tomography techniques [4] have reported reduced glucose metabolism in the striatum and declined nigrostriatal dopaminergic neural transmission function in both the presynaptic and postsynaptic sites. No pathological or neuroimaging studies, however, have examined the relationship between the degeneration/dysfunction of nigrostriatal presynaptic and postsynaptic dopaminergic systems. It is well known that responses to L-3,4,dihydroxyphenyl-alanine (L-DOPA) are generally poor in MSA [1], and this is ascribable to the fact that the pathology of MSA involves not only SN but also the striatum where the dopamine receptors exist. A transient effect, however, is occasionally noted in the early stages in certain cases. Wenning *et al.* [5] proposed a hypothesis based on the pathological finding of a dissociation between the SN and striatal degeneration that may account for such L-DOPA responsiveness. No pathological or neuroimaging evidence that directly demonstrated the dissociation in such cases, however, has been found.

We simultaneously measured the presynaptic and postsynaptic nigrostriatal dopaminergic functions using PET in MSA-P patients, including L-DOPA-responsive cases, and the regional correlation of two parameters was analyzed in the striatum to examine the characteristics of the disease and the mechanisms of L-DOPA responsiveness.

Methods

This study was approved by the Ethical Committee of Tokyo Metropolitan Institute of Gerontology. The objective and effect of the PET examination on the human body were adequately explained to all participants, and written informed consent was obtained.

Participants

We studied eight patients (68.9 ± 7.4 years old) clinically diagnosed as MSA-P according to the consensus criteria established by Gilman *et al.* [6] (Table 1). The MSA-P patients underwent PET examination following a 15-h deprivation of antiparkinsonian drugs. The primary symptom observed in all the patients was parkinsonism; further, during the course of the disease, parkinsonism was noted to be the cardinal symptom. Magnetic resonance imaging

Table 1 Clinical features of the eight patients with the parkinsonian phenotype of multiple system atrophy

Patient no./age (years)/sex	Hoehn and Yahr stage	Disease duration (years)	Autonomic dysfunction	Cerebellar dysfunction	Pyramidal sign	MRI findings	L-DOPA response
1/79/Female	III	1	+	+	+	Put	+
2/73/Female	III	1	+	+	+	Put	+
3/66/Female	I	2	+	+	+	No findings	–
4/61/Female	IV	2	+	+	+	cbll/put	–
5/72/Male	V	3	+	–	+	Put	–
6/56/Male	IV	4	+	+	+	Pons/cbll/put	–
7/73/Female	III	6	+	+	+	Pons/cbll/put	–
8/71/Female	V	9	+	–	+	Put	–

Signal change in the pons/middle cerebellar peduncles includes pontine/cerebellar atrophy (pons/cbll); Slit-like signal change at the posterolateral putaminal margin includes putaminal atrophy (put).L-DOPA, L-3,4,dihydroxyphenyl-alanine.

(MRI) examination was also performed. The characteristics of the patients are presented in Table 1. Among the eight cases of MSA-P, cases 1 and 2 apparently responded to L-DOPA at the time of the PET study, and the improvement in the symptoms of parkinsonism due to L-DOPA was confirmed by neurologists.

The healthy control group consisted of eight participants (five men and three women, 62.3 ± 6.9 years old) that did not have a past medical history of neurological and psychiatric disorders. They were diagnosed as normal after physical and neurological examinations, screening MRI scans, and Mini-Mental Scale Evaluation (>28). They had not taken any neuroleptic drugs and were not addicted to alcohol; no history of any other substance abuse was present.

Positron emission tomography scans

^{11}C-labeled 2β-carbomethoxy-3β-(4-fluorophenyl)-tropane ([^{11}C]CFT) as a marker of presynaptic dopaminergic function for dopamine transporters and ^{11}C-labeled raclopride ([^{11}C]RAC) as a marker of postsynaptic dopaminergic function for dopamine D_2-like receptors were used as tracers for PET [7,8]. The methods used for the preparation of the radiopharmaceuticals were as described previously [9,10].

All the participants underwent the two PET studies on the same day with a 3–4-h interval. PET images were acquired in three-dimensional mode using the SET-2400W (Shimadzu, Kyoto, Japan) scanner [11] at the Positron Medical Center, Tokyo Metropolitan Institute of Gerontology. The acquired PET images were 128 × 128 × 50 in matrix size with a 2 × 2 × 3.125-mm voxel size. In PET acquisition, 300 MBq each of [^{11}C]CFT and [^{11}C]RAC were administered by an intravenous bolus injection, and all participants rested in a supine position with their eyes open during the test. The specific activity and the amount of cold material injected were 5.4–47 MBq/nM and 1.2–8.6 nM, respectively, for [^{11}C]CFT and 10–130 MBq/nM and 0.42–3.1 nM, respectively, for [^{11}C]RAC. For three of the eight healthy control participants, a dynamic scan was performed for 90 min for the [^{11}C]CFT study in the morning and for 60 min for the [^{11}C]RAC study in the afternoon to estimate the binding potentials. To measure the uptakes of these two tracers, for the five healthy participants and all the patients, a static scan was performed 75–90 min after the injection of the [^{11}C]CFT and 40–55 min after the injection of [^{11}C]RAC, respectively. The attenuation was corrected by a transmission scan using a ^{68}Ga/^{68}Ge source.

Data analysis

The two PET images of the [^{11}C]CFT and [^{11}C]RAC examinations obtained from the same participant were coregistered using an automated image registration program [12]. The images were processed further using Dr View software (AJS, Tokyo, Japan) on Linux workstations. Next, the images were resliced in the transaxial direction parallel to the anterior–posterior intercommissural (AC-PC) line, and the regions of interest (ROIs) were placed on the three subregions of the striatum – the bilateral caudate nuclei, anterior putamen, and posterior putamen – in two slices, that is, the AC-PC plane and 3.1 mm above the AC-PC line. ROIs of the striatum consisted of circles of 8-mm diameter. On each side of each slice, we set one ROI in the caudate and two ROIs each in the anterior and posterior putamen. The reference regions of the occipital lobe were placed in four slices in a range of 12.5–21.9 mm above the AC-PC plane. The reference region of the occipital lobe consisted of circles of 10-mm diameter, and we set four such circles on each side of each slice.

First, for dynamic scan data, the binding potential of the tracer in the bilateral caudate nuclei, anterior putamen, and posterior putamen of three healthy participants was estimated by a simplified reference region model [13] using the occipital lobe as a reference. Second, for static imaging, the uptake ratio index (URI) was calculated for all participants by the following formula:

$$\mathrm{URI} = (\mathrm{Activity}_{\mathrm{Striatumsubregion}} - \mathrm{Activity}_{\mathrm{Occipitallobe}})/\mathrm{Activity}_{\mathrm{Occipitallobe}})$$

URI was also calculated for the dynamic scan in the three healthy control participants using the data obtained from an equivalent time-frame. The URI in each ROI was compared between MSA-P patients and control participants with the Mann–Whitney *U*-test with Bonferroni's correction for multiple comparisons.

Next, we examined the correlation between the binding potential and the URI.

Results

For each tracer, the URIs of the striatal subregions in the static image were linearly correlated with the binding potentials in the dynamic scan (r^2=0.92, P<0.0001 for [^{11}C]CFT and r^2=0.93, P<0.0001 for [^{11}C]RAC). Therefore, we adopt the URI in reference to the occipital cortex for the further analysis.

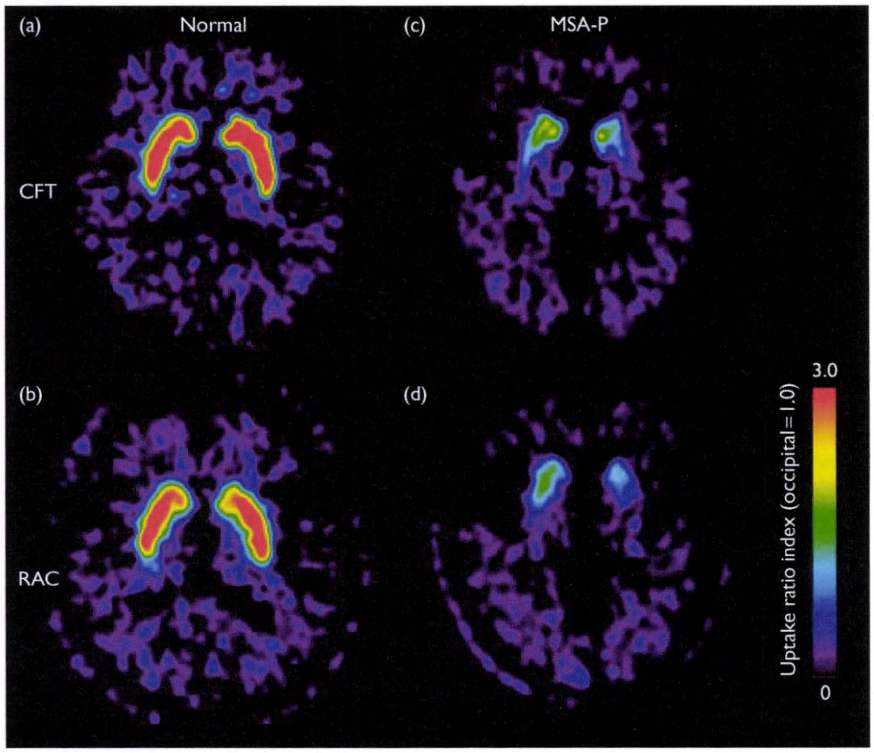

Fig. 1 Positron emission tomography images. (a) [^{11}C]CFT and (b) [^{11}C]RAC images were obtained from a normal participant, and (c) [^{11}C]CFT and (d) [^{11}C]RAC images were obtained from an MSA-P patient. All the images were normalized to the occipital lobe activity and obtained in a +3.1-mm plane from the anterior–posterior intercommissural line. [^{11}C]CFT, ^{11}C-labeled 2β-carbomethoxy-3β-(4-fluorophenyl)-tropane; [^{11}C]RAC, ^{11}C-labeled raclopride; MSA-P, phenotype of multiple system atrophy.

Table 2 The uptake ratio index of [^{11}C]CFT and [^{11}C]RAC in the subregions of the striatum

	Normal participants (n=8)	MSA-P patients (n=8)	Percentage of control
Caudate			
[^{11}C]CFT	3.70±0.55	2.49±0.41*	67.3
[^{11}C]RAC	3.46±0.40	2.63±0.31*	76.0
Anterior putamen			
[^{11}C]CFT	4.04±0.45	1.97±0.45*	48.8
[^{11}C]RAC	3.97±0.31	2.46±0.46*	62.0
Posterior putamen			
[^{11}C]CFT	3.82±0.47	1.58±0.42*	41.4
[^{11}C]RAC	3.90±0.32	2.07±0.67*	53.1

*P<0.05 as compared with normal controls (Mann–Whitney U-test with Bonferroni's multiple comparison correction).
[^{11}C]CFT, ^{11}C-labeled 2β-carbomethoxy-3β-(4-fluorophenyl)-tropane; [^{11}C]RAC, ^{11}C-labeled raclopride; MSA-P, phenotype of multiple system atrophy.

Figure 1 demonstrates the representative PET images of a normal participant and an MSA-P patient. In the MSA-P patient, the URIs of both [^{11}C]CFT and [^{11}C]RAC declined in the striatum compared with the normal participant (Fig. 1).

The results of ROI measurement are summarized in Table 2. In the MSA-P group, the URIs of both [^{11}C]CFT and [^{11}C]RAC significantly decreased in all the subdivisions of the striatum (P<0.05) in comparison with the control group, and the decrease was most prominent in the posterior putamen and relatively smaller in the caudate nuclei.

Scatter plots of the entire uptake data in individual participants for each of the three regions are shown in Fig. 2a–c and those for all areas are shown in Fig. 2d. A strong positive correlation was noted between the URIs of [^{11}C]CFT and [^{11}C]RAC in the MSA-P group. That is, the impairment of presynaptic and postsynaptic nigrostriatal dopaminergic function was observed in associative degree in all the subregions of the striatum.

Two patients apparently responded to the L-DOPA administration at the time of PET studies. Figure 2 indicates that the decrease in the [^{11}C]RAC uptake was relatively lesser in comparison with that in the [^{11}C]CFT uptake in the L-DOPA-responsive cases.

Discussion

In earlier studies, the cerebellum has been widely used as a reference region to estimate the availability of dopamine transporters using [^{11}C]CFT [14,15] and dopamine D_2-like receptors using [^{11}C]RAC [16]. We, however, selected the occipital cortex as a reference region in this study. Neuropharmacological evidence has revealed that the densities of both the dopamine transporters and dopamine D_2-like receptors in the human occipital cortex are negligible as in the case of the cerebellum [17]. Furthermore, the cerebellum is often involved in the pathological processes in MSA-P, whereas the occipital lobe is less likely to be affected. The selection of the occipital region as a reference would be useful for PET analysis of MSA. In contrast, the measured values of the striatum might have affected by the atrophy. The correlation of two PET measures on the same regions, however, are robust because they are evaluated with common ROIs to cancel out the spatial effect.

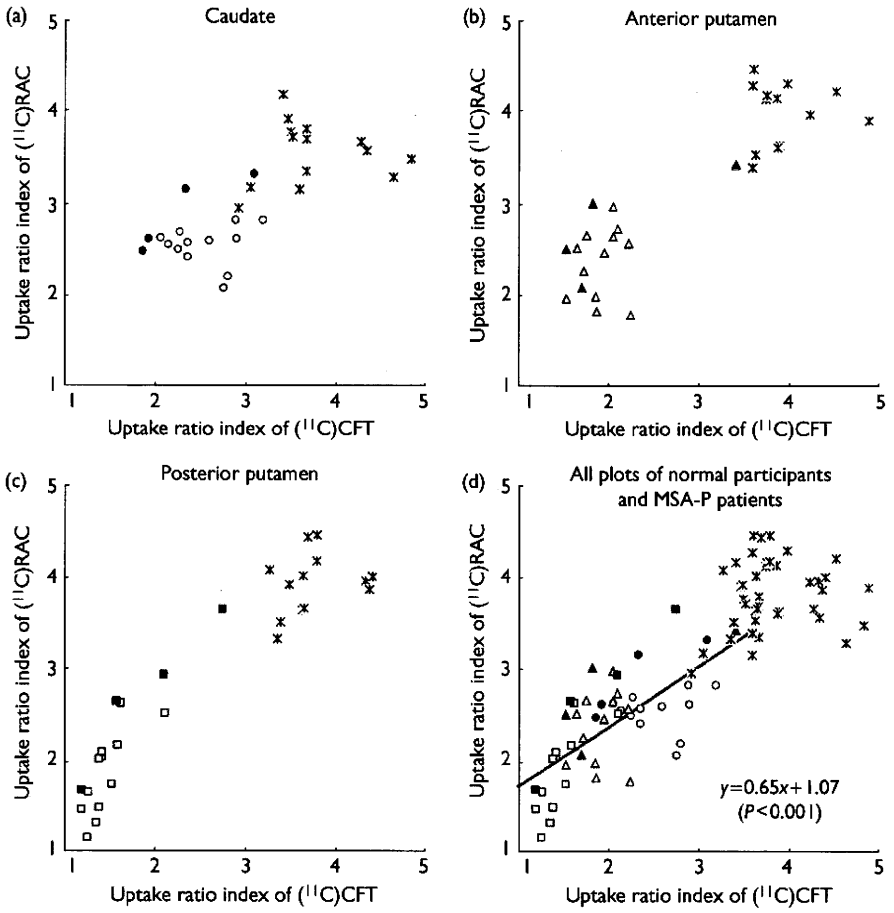

Fig. 2 The correlation between the uptake ratio index (URI) of [^{11}C]CFT and that of [^{11}C]RAC in the caudate nuclei (a), anterior putamen (b), posterior putamen (c), and all these areas (d) of all participants including MSA-P patients (n=8) and normal participants (n=8). The approximate lines for all the plots of the MSA-P group are shown in (d). Asterisk (*), normal participants; open circles (○), the caudate nuclei in MSA-P patients; open triangles (Δ), the anterior putamen in MSA-P patients; open squares (□), the posterior putamen in MSA-P patients; and solid markers (●), MSA-P patients exhibiting L-DOPA responsiveness. [^{11}C]CFT, ^{11}C-labeled 2β-carbomethoxy-3β-(4-fluorophenyl)-tropane; [^{11}C]RAC, ^{11}C-labeled raclopride; L-DOPA, L-3,4,dihydroxyphenyl-alanine; MSA-P, phenotype of multiple system atrophy.

Using [^{11}C]CFT and [^{11}C]RAC, we simultaneously measured presynaptic and postsynaptic nigrostriatal dopaminergic functions and observed that both functions were significantly impaired in all eight patients with MSA-P compared with the normal group.

The functional impairment in the striatum was more noticeable in the putamen, particularly in its posterior part, than in the caudate nuclei. The most prominent result of our study was that a strong positive correlation was noted between presynaptic and postsynaptic functional impairments in the MSA-P group throughout the striatum regardless of the severity of the impairments. In Parkinson's disease (PD), presynaptic and postsynaptic functional impairments were reported to be negatively correlated in the putamen by PET using [^{11}C]CFT and [^{11}C]SCH 23390 (dopamine D_1-like receptor probe), reflecting severe impairment in the presynaptic marker with an upregulation of the postsynaptic function [18]. The differential diagnosis between MSA-P and PD in clinical situations is at times difficult. The patterns of presynaptic and postsynaptic functional impairments, however, demonstrated by PET contrasted between MSA-P and PD, and therefore the two disorders can be clearly differentiated with combined presynaptic and postsynaptic dopaminergic PET examinations.

Ghaemi *et al.* [3] applied PET using [^{18}F]FDOPA and [^{11}C]RAC to MSA-P patients and discovered that both presynaptic and postsynaptic dopaminergic functions were reduced in the nigrostriatal dopaminergic system. They did not, however, provide information about whether the impairments in the presynaptic and postsynaptic dopaminergic function were correlated in each participant. Our study is the first to demonstrate a positive correlation between the presynaptic and postsynaptic dopaminergic function with respect to the local subdivisions of the striatum and the disease duration.

What is the pathological background of the strong correlation of presynaptic and postsynaptic markers measured by PET? Pathologically, neuronal loss and gliosis are the primary forms of impairment in MSA [2]. The neuronal loss tends to be severe in both SN and striatum; however, it is not always to the same extent [1], and there has been no report regarding the correlation of pathological findings such as glial cytoplasmic inclusion [19] and α-synuclein

[20,21] between SN and striatum. If the PET markers for presynaptic and postsynaptic dopaminergic function directly reflect the degree of degeneration in SN and striatum independently, as in PD [15,22], the combination in the degree of presynaptic and postsynaptic functional impairment could be variable. The presence of a strong positive correlation between the presynaptic and postsynaptic dopaminergic functions measured by PET within participants and across participants suggests that these impairments in MSA-P are the result of the destruction of the entire synaptic structure in the striatum. Pathologically, the putamen is one of the areas with the most severe neuronal loss in MSA-P [2]. We consider that the presynaptic marker represents the degree of degeneration of the SN only if the striatum involvement is lesser than that of SN; however, once the severe destruction of striatum occurs, the presynaptic marker no longer represents the degree of SN degeneration because it is masked by the destruction of the entire structure of the synapse.

Parkinsonism in MSA is treated with L-DOPA, dopamine agonists, and anticholinergic agents; however, only a mild effect is noted in a minor population in the early stage, and the responsiveness to L-DOPA gradually disappears. Generally, responses to L-DOPA are poor in cases of MSA-P [1]. In a previous report, L-DOPA was effective in the early stage in approximately 1/3 of the MSA cases [23]. We examined two early MSA-P cases responsive to L-DOPA. In these cases, the presynaptic dopaminergic function was markedly reduced; however, the reduction in the postsynaptic dopaminergic function was relatively less severe compared with that in the cases not responsive to L-DOPA; moreover, this trend was more prominent in the striatum on the contralateral side in which L-DOPA alleviated the symptoms of parkinsonism. Churchyard *et al.* [24] suggested that the ineffectiveness of L-DOPA on parkinsonism in MSA is related to the dominance of neuronal loss, gliosis, and the reduction in postsynaptic dopamine D_2 receptors in the posterior putamen. Wenning *et al.* [5] reported that L-DOPA was highly effective in the cases in which the putamen was relatively conserved compared with the degree of nigral neuronal loss, and the effect of L-DOPA was negatively correlated with the degree of nigral degeneration, suggesting that nigral degeneration precedes striatal degeneration [1]. Whether nigral degeneration preceded striatal degeneration was not clear in our study; however, postsynaptic dopaminergic function was relatively retained in our L-DOPA-responsive cases. We consider that the degree of conservation of postsynaptic dopaminergic function is related to the effectiveness of L-DOPA in MSA-P and that a trend of dissociation of presynaptic and postsynaptic markers can be detected by PET. Further studies are necessary to increase the number of the participants and to follow up the L-DOPA-responsive cases using PET and clinical course observations.

Conclusion

We have established the presence of a strong positive correlation between the reductions in nigrostriatal presynaptic and postsynaptic dopaminergic functions and L-DOPA-responsive cases in which the degrees of presynaptic and postsynaptic functional impairments are dissociated in some manner.

The elucidation of the patterns and processes of presynaptic and postsynaptic functional impairments may provide a clue to understanding the development and advancement mechanisms of the disease and will aid in a more reliable early clinical diagnosis and prediction of drug effects.

References

1. Wenning GK, Ben-Shlomo Y, Magalhaes M, Daniel SE, Quinn NP. Clinicopathological study of 35 cases of multiple system atrophy. *J Neuro Neurosurg Psychiatry* 1995; **58**:160–166.
2. James SL, Nigel L. Disorders of movement and system degeneration. In: David IG, Peter LL, editors. *Greenfield's neuropathology.* 7th ed. Vol. 2. London: Arnold; 2002. pp. 325–430.
3. Ghaemi M, Hilker R, Rudolf J, Sobesky J, Heiss WD. Differentiating multiple system atrophy from Parkinson's disease: contribution of striatal and midbrain MRI volumetry and multi-tracer PET imaging. *J Neurol Neurosurg Psychiatry* 2002; **73**:517–523.
4. Van Royen E, Verhoeff NF, Speelman JD, Wolters EC, Kuiper MA, Janssen AG. Multiple system atrophy and progressive supranuclear palsy. Diminished striatal D_2 dopamine receptor activity demonstrated by ^{123}I-IBZM single photon emission computed tomography. *Arch Neurol* 1993; **50**:513–516.
5. Wenning GK, Quinn N, Magalhaes M, Mathias C, Daniel SE. 'Minimal change' multiple system atrophy. *Mov Disord* 1994; **9**:161–166.
6. Gilman S, Low P, Quinn N, Albanese A, Ben-Shlomo Y, Fowler C, *et al.* Consensus statement on the diagnosis of multiple system atrophy. American Autonomic Society and American Academy of Neurology. *Clin Auton Res* 1998; **8**:359–362.
7. Volkow ND, Fowler JS, Gatley SJ, Logan J, Wang GJ, Ding YS, *et al.* PET evaluation of the dopamine system of human brain. *J Nucl Med* 1996; **37**:1242–1256.
8. Booij J, Tissingh G, Winogrodzka A, van Royen EA. Imaging of the dopaminergic neurotransmission system using single-photon emission tomography and positron emission tomography in patients with parkinsonism. *Eur J Nucl Med* 1999; **26**:171–182.
9. Kawamura K, Oda K, Ishiwata K. Age-related changes of the [^{11}C]CFT binding to the striatal dopamine transporters in the Fischer 344 rats: a PET study. *Ann Nucl Med* 2003; **17**:249–253.
10. Langer O, Någren K, Dolle F, Lundkvist C, Sandell J, Swahn CG, *et al.* Precursor synthesis and radiolabelling of the dopamine D_2 receptor ligand [^{11}C]raclopride from [^{11}C]methyl triflate. *J Labelled Comp Radiopharm* 1999; **42**:1183–1193.
11. Fujiwara T, Watanuki S, Yamamoto S, Miyake M, Seo S, Itoh M, *et al.* Performance evaluation of a large axial field-of-view PET scanner : SET-2400W. *Ann Nucl Med* 1997; **11**:307–313.
12. Ardekani BA, Braun M, Hutton BF, Kanno I, Iida H. A fully automatic multimodality image registration algorithm. *J Comput Assist Tomogr* 1995; **19**:615–623.
13. Gunn RN, Lammertsma AA, Hume SP, Cunningham VJ. Parametric imaging of ligand-receptor binding in PET using a simplified reference region model. *NeuroImage* 1997; **6**:279–287.
14. Wong DF, Yung B, Dannals RF, Shaya EK, Ravert HT, Chen CA, *et al.* In vivo imaging of baboon and human dopamine transporters by positron emission tomography using [^{11}C]WIN 35 428. *Synapse* 1993; **15**:130–142.
15. Frost JJ, Rosier AJ, Reich SG, Smith JS, Ehlers MD, Snyder SH, *et al.* Positron emission tomographic imaging of the dopamine transporter with ^{11}C-WIN 35,428 reveals marked declines in mild Parkinson's disease. *Ann Neurol* 1993; **34**:423–431.
16. Antonini A, Leenders KL, Reist H, Thomann R, Beer HF, Locher J. Effect of age on D_2 dopamine receptors in normal human brain measured by positron emission tomography and ^{11}C-raclopride. *Arch Neurol* 1993; **50**:474–480.
17. Mozley PD, Stubbs JB, Kung HF, Selikson MH, Stabin MG, Alavi A. Biodistribution and dosimetry of iodine-123-IBF: a potent radioligand for imaging the D2 dopamine receptor. *J Nucl Med* 1993; **34**:1910–1917.
18. Ouchi Y, Kanno T, Okada H, Yoshikawa E, Futatsubashi M, Nobezawa S, *et al.* Presynaptic and postsynaptic dopaminergic binding densities in the nigrostriatal and mesocortical systems in early Parkinson's disease: a double-tracer positron emission tomography study. *Ann Neurol* 1999; **46**:723–731.